Heading

Host-induced gene silencing involves transfer of dsRNA-derived siRNA via extracellular vesicles

Koch A[1*], Schlemmer T[1*], Höfle L[1*], Werner BT[1], Preußer C[2], Hardt M[3], Möbus A[3], Biedenkopf D[1], Claar M[1], Perlet C[1], Jelonek L[4], Goesmann A[4], Garikapati V[5], Spengler B[5], Busche T[6], Kalinowski J[6], Kogel KH[1]

[1]Institute of Phytopathology, Centre for BioSystems, Land Use and Nutrition, Justus Liebig University, Heinrich-Buff-Ring 26, D-35392, Giessen, Germany

[2]Institute of Biochemistry, Justus Liebig University, Heinrich-Buff-Ring 17, D-35392, Giessen, Germany

[3]Biomedical Research Centre Seltersberg (BFS), Imaging Unit, Justus Liebig University, Schubertstraße 81, D-35392, Giessen, Germany

[4]Institute of Bioinformatics and Systems Biology, Justus Liebig University, Heinrich-Buff-Ring 58, D-35392, Giessen, Germany

[5]Institute of Inorganic and Analytical Chemistry, Justus Liebig University, Heinrich-Buff-Ring 17, D-35392, Giessen, Germany

[6]Centre for Biotechnology - CeBiTec, Bielefeld University, Universitätsstraße 25, D-33615, Bielefeld, Germany

*shared first authorship

Email addresses

Aline.Koch@agrar.uni-giessen.de

Karl-Heinz.Kogel@agrar.uni-giessen.de

Correspondence to

Aline.Koch@agrar.uni-giessen.de

Abstract

Small (s)RNA molecules are crucial factors in the communication between hosts and their interacting pathogens, where they function as effectors that can modulate both host defense and microbial virulence/pathogenicity through a mechanism termed cross-kingdom RNA interference (ckRNAi). Consistent with this recent knowledge, sRNAs and their double-stranded (ds)RNA precursors have been adopted to control diseases in crop plants through transgenic expression (host-induced gene silencing, HIGS) or exogenous application (spray-induced gene silencing, SIGS). While these strategies proved to be effective, the mechanism of RNA transfer at the plant - pathogen interface is widely unresolved. Here we show that extracellular vesicles (EVs) purified from Arabidopsis (*Arabidopsis thaliana*) leaf extracts and apoplastic fluids contain transgene-derived sRNAs. EVs from plants expressing CYP3RNA, a 791 nt long dsRNA, which was originally designed to target the three *CYP51* genes of the fungal pathogen *Fusarium graminearum*, contain CYP3RNA-derived small interfering (si)RNAs as shown by RNA sequencing (RNA-seq) analysis. Notably, the EVs cargo retained the same CYP3RNA-derived siRNA profile as the respective leaf extracts, suggesting that there was no selective uptake of specific artificial sRNAs into EVs. In addition, mutants of the ESCRT-III complex were impaired in HIGS further indicating that endosomal vesicle trafficking supports transfer of transgene-derived siRNAs between donor host cells and recipient fungal cells. Further supporting the relevance of EV-mediated transport of sRNA, we demonstrate that HIGS plants, expressing a 100 nt dsRNA-target-sequence identified via EV-sRNA-seq of CYP3RNA Arabidopsis, confers strong resistance to *F. graminearum*. Together, these findings support the view that EVs are key mediators in the transport of HIGS-related sRNAs to reduce the virulence of interacting fungal pathogens during host-pathogen interaction.

Introduction

Small (s)RNA effectors play a crucial role in the outcome of plant-pathogen interactions [1-4] and have a great potential for controlling diseases and pests in crop plants [5-8] A multitude of transgenic crops expressing dsRNAs targeting essential genes through RNAi are more resistant to viruses [9], viroids [10], bacteria [11], fungi [12-15], oomycetes [16], nematodes [17,18], and insects [19,20]. Host-induced gene silencing (HIGS) involves *i.* processing of transgene-derived dsRNA into small interfering (si)RNAs, *ii.* siRNA transfer into the interacting microbe/pest, and *iii.* siRNA interference with their target transcripts, though many details of the process have not been fully elucidated. Several reports suggested to use exogenous RNA to control fungal diseases [21-25]. In the case of spray-induced gene silencing (SIGS) both the plant and the microbe silencing machinery appears to contribute to inhibition of the fungus [25]. Despite the promising prospective for RNAi-based disease control in agriculture, little is known about the mechanisms underlying the transport of RNAs from the plant host to an interacting microbial pathogen. While nematodes and some insects possess a transmembrane channel-mediated RNA uptake mechanism for intake and cell-to-cell distribution based on *Caenorhabditis elegans* SID proteins (SYSTEMIC RNA INTERFERENCE DEFICIENT) [26], fungi and plants lack these proteins. Alternatively, it has been hypothesized that plant sRNA effectors are associated with RNA-binding proteins (RBPs) and/or extracellular vesicles (EVs) [22,27,28]. The interface between a plant and an interacting fungus is the primary site for mutual recognition, where vesicle secretion from both organisms occurs [29-31]. Several types of EVs, defined according to size and origin, have been identified in eukaryotic cells [32]. The largest class are apoptotic bodies with diameters of 800-5,000 nm. They are released by cells undergoing programmed cell death, thus reflecting the initially anticipated role of EVs as waste disposal system. EVs within a size range of 100-1,000 nm are categorized as large EVs that are released by budding from the plasma membrane (PM), while endosome-derived small EVs instead are only 30-200 nm in diameter and are released when multivesicular bodies

(MVBs) fuse with the PM [33-37]. In mammals, exosomes mediate intercellular communication by shuttling proteins, lipids and RNAs, where RNA molecules remain functional after delivery and can elicit effects in the recipient cell [38-40].

Based on this knowledge, we speculated that HIGS- and SIGS-related RNAs also are loaded into plant vesicles and transferred by EVs that cross the plant-fungus interface. It was reasoned already more than 50 years ago that a fusion of plant MVBs with the PM may result in the release of small vesicles into the extracellular space [41]. Consistent with this early observation, biogenesis of immune-related MVBs [29,30] and the release of their cargo via EVs also is inherent to the plant secretory pathway [27]. Transmission electron microscopy (TEM) revealed proliferation of MVBs next to plant cell wall papillae in response to infection with powdery mildew fungus and the release of para-mural vesicles. The authors proposed that released vesicles might be similar to exosomes in animal cell thus anticipating that exosomes exist in plants [29,30]. Immune-related plant EVs may carry defence compounds to strengthen the plant cell wall at the site of fungal attack. Supporting this notion, proteins, hydrogen peroxide, and callose could be identified inside MVBs next to the PM [30,42]. EVs also were identified in the extrahaustorial matrix of powdery mildew fungus, though it could not be determined whether these vesicles were of plant or fungal origin [43].

Rutter and Innes [27] isolated EVs from endosomal origin in a size range of 50-300 nm from the apoplast of Arabidopsis leaves, thus providing a direct proof that exosomes also exist in plants. Vesicle secretion was enhanced in response to either the bacterial pathogen *Pseudomonas syringae* or the defence signalling compound salicylic acid. Consistent with this, the EV proteome was enriched for proteins associated with abiotic and biotic stress responses, including proteins involved in signal transmission, such as RPM1-INTERACTING 4 (RIN4), proteins of the myrosinase-glucosinolate system, such as the glucosinolate transporters PENETRATION 3 (PEN3) shown to accumulate around powdery mildew haustoria [44], proteins involved in reactive oxygen species (ROS) signaling and oxidative stress responses,

proteins involved in membrane-trafficking, among them syntaxins such as PEN1, and proteins for the transport of ions, water, and sugar substrates. Moreover, EVs contained other trafficking proteins such as RAB GTPases and PATELLIN 1 and 2 (PATL1 and PATL2). PATL1 and PATL2 bind phosphoinositides and mediate vesicle transport and/or fusion [45]. PATL1 localizes to the cell plate in dividing cells but also associates with PLASMODESMATA-LOCATED PROTEIN1 (PDLP1) during downy mildew infection and may colocalize with PDLP1 at the extrahaustorial membrane [46].

Here we assess whether artificial, antifungal dsRNA originating either from an endogenous transgene or exogenous spray application are incorporated into plant EVs. We show that EVs from leaves of transgenic Arabidopsis plants expressing CYP3RNA, a 791 nts long noncoding dsRNA that concomitantly silences the two fungal cytochrome P450 sterol 14α-demethylase genes *CYP51A* and *CYP51B* and the virulence factor *CYP51C* and inhibits the growth of *Fusarium graminearum* (*Fg*) both *in vitro* and *in planta* [12,25,47], contain CYP3RNA-derived siRNAs. Moreover, mutants of secretory vesicle pathway showed a loss of HIGS-mediated resistance. Of note, our data suggest that SIGS-mediated resistance against *Fg* was independent of EVs suggesting mechanistic differences between the two delivery strategies. Finally, we confirmed the antifungal activity of the EV cargo, when generating HIGS plants expressing a highly-targeted 100 nt dsRNA identified by EV-sRNA-seq analysis. This construct exhibited similar *Fg* disease resistance as the original 791 nt CYP3RNA construct.

Results

Exosome-like vesicles from leaf extracts of CYP3RNA-expressing transgenic Arabidopsis contain CYP3RNA-derived siRNAs

The present knowledge on plant EVs is consistent with the idea of an EV-mediated effector shuttle in ckRNAi [1,22,48-55]. Here, we tested the possibility that HIGS also involves vesicle transport of dsRNA-derived sRNAs. To this end, we isolated vesicles from plants expressing

the 791 nt CYP3RNA that was previously shown to confer resistance against *Fg* by silencing the three fungal genes *FgCYP51A*, *FgCYP51B* and *FgCYP51C* [12,25,47]. After differential centrifugation of the leaf cell extract (see MM), vesicles were pelleted by 160,000 xg ultracentrifugation and subsequently loaded on top of a sucrose density gradient. Subsequent to an additional ultracentrifugation step, two green coloured bands in the gradients of samples from wt and CYP3RNA-expressing plants contained vesicles (Figure 1(a)(b)). The upper band (fraction F160-s1), located between the 30% and 45% sucrose layer, and the lower band (fraction F160-s2), located between the 45% and 60% layer, were harvested separately and inspected by negative staining and TEM. Fractions F160-s1 contained vesicles that were in a size range of about 50 nm to 200 nm. Most of them were cup-shaped and surrounded by a layer reminiscent of a membrane. Fractions F160-s2 contained only a few vesicles and most of them were not surrounded by a membrane (Supplementary Figure 1(a)), while the fraction between the two visible greenish bands was mainly free of vesicles (Supplementary Figure 1(b)). The size of the vesicles from the upper fraction was further determined using ImageJ, revealing an average diameter of about 95 nm for wt plants and 105 nm for CYP3RNA-expressing plants (Table 1). This size fits with the size definition of mammalian small EVs having 30 nm to maximal 150 nm in diameter and Arabidopsis EVs having 50 nm to maximal 300 nm in diameter [27,37].

Next, we assessed whether vesicles from leaf extracts of transgenic Arabidopsis contain RNA derived from the CYP3RNA precursor. Vesicles from the F160-s1 fraction were washed in 1x phosphate buffer saline (PBS), pelleted by 160,000 x*g* and RNA extraction was performed subsequently, with a final profiling of the sRNA by RNA-seq (sRNA-seq). Vesicles of the F160-s1 fractions yielded 720 ng (CYP3RNA plants) and 1,080 ng (wt plants) RNA, respectively, (purified each from 120 leaves (Supplementary Table 1)). Indexed sRNA libraries were constructed, pooled and sequenced on an Illumina MiSeq Platform, resulting in 5.3 and 2.1 million reads from libraries of CYP3RNA-expressing and wt plants, respectively

(Supplementary Table 2). By mapping reads to the CYP3RNA precursor sequence, we found 31 unique siRNAs with lengths ranging from 21 to 24 nts (Figure 1(c)(d)) aligning to CYP3RNA, while no CYP3RNA matching reads were found in vesicles from wt plants (Supplementary Figure 2). Overall only 79,223 reads out of 5.3 million total reads from CYP3RNA plants were small RNAs (21 to 24 nts in length) which can be explained by the fact that total vesicle RNA was not size fractionated before sequencing. From the 31 siRNAs (total reads: 442 rpm) mapping to the CYP3RNA precursor sequence, 12 siRNAs (total reads: 177 rpm) matched the CYP51A fragment, 10 siRNAs (total reads: 126 rpm) matched the CYP51B fragment, and five siRNAs (88 rpm) matched the CYP51C fragment. Interesting to note, slightly more siRNAs matched to the CYP51A fragment which is located in the middle of the CYP3RNA sequence (Figure 1(e); Supplementary Figure 3).

EVs from apoplastic fluids of transgenic Arabidopsis contain CYP3RNA-derived siRNA

The findings above show that siRNAs from a dsRNA precursor transgene are incorporated into plant vesicles. To further substantiate this finding, we isolated EVs from extracellular washing fluids of CYP3RNA-expressing and wt Arabidopsis plants, following a published protocol [27]. Whole rosettes of 5-wk-old Arabidopsis plants were vacuum infiltrated with vesicle isolation buffer (VIB) until infiltration sites were visible as dark green leaf areas. After gathering apoplastic fluid by low speed centrifugation, vesicles were isolated by differential centrifugation at 48,000 x*g* (F48) and 100,000 x*g* (F100). Pellets from the centrifugation steps were analysed by TEM. Consistent with the earlier report [27], the F48 fraction contained vesicle-like structures resembling EVs in size and shape (Figure 2a)). While the shape and structure of these vesicles were otherwise indistinguishable from vesicles isolated by sucrose gradient. Analysis of the particle diameter using ImageJ revealed an average diameter of about 141 nm and 119 nm for CYP3RNA-expressing and wt plants, respectively (see Table 1). This fits well with the observation of Rutter and Innes [27] showing that the most abundant particles

in the F48 fraction had around 150 nm in diameter as detected by light-scattering. Also consistent with the above report, the F100 fraction was mostly devoid of vesicles and instead contained a multitude of small particles with diameters under 30 nm (Figure 2(b)). We further analysed the size of EVs by nanoparticle tracking analysis (NTA). We found an EV average size of 139 +/- 7.7 nm (Figure 2(c); Supplementary Figure 4). To further substantiate that the F40 fraction contains EVs, we conducted an immunoblot analysis detecting the membrane marker PEN1 [27]. We found a strong signal for PEN1 in extracts from the F40 fractions (Figure 2(d)).

Next, we assessed the RNA cargo of EVs of the F48 fraction. Before RNA extraction, EVs were treated with 0.4 ng μL^{-1} RNase for 10 min at 37°C in PBS to digest extravesicular RNA. From infiltration of 10 plants we gained 90 ng (CYP3RNA plants) and 30 ng (wt plants) RNA, respectively (Supplementary Table 1). Subsequently, RNA was subjected to sRNA-seq (Supplementary Table 2). Mapping of siRNA reads to the CYP3RNA precursor identified 607 rpm (58 unique) CYP3RNA-matching siRNAs (Figure 2(e)), while no specific reads were detected in the EVs from apoplastic fluids of Arabidopsis wt leaves (Supplementary Figure 5). Like RNA cargo of vesicles from leaf extracts, siRNA sizes from 21 to 24 nts (Figure 2(f)) mapped to all three *FgCYP51* gene fragments in the CYP3RNA precursor (Figure 2(e)). Notably, we found CYP3RNA-derived siRNAs showing a bias towards a 5'-uracil (U) and 5'-adenine (A), while the total sRNAs from wt plants and CYP3RNA plants showed no obvious bias towards a specific 5'nuleotide (Figure 2(g)). From the total of 58 siRNA (607 rpm) mapping to CYP3RNA, 24 unique siRNAs (total reads: 242 rpm) mapped to the CYP51A fragment, four unique siRNAs (total reads: 31 rpm) mapped to the CYP51B fragment, and 19 siRNAs (total reads: 180 rpm) mapped to the CYP51C fragment, substantiating the slight bias for siRNAs matching the CYP51A fragment. We further assessed whether the slight bias for CYP51A-matching siRNAs is reflected in the whole cell extracts or is a characteristic of the vesicle cargo. To this end, total leaf sRNA of CYP3RNA-expressing Arabidopsis was

sequenced. As in vesicles, we found a bias for CYP51A-targeting siRNAs (Figure 3(a)(b)), suggesting that the uptake of siRNAs into vesicles is non-selectively for CYP3RNA-derived siRNAs.

Transgenic Arabidopsis plants expressing a highly-targeted 100 nt sequence of *FgCYP51A* (Hotspot-A-dsRNA) are resistant to *Fg*

RNA-seq profiles of EVs and whole leaves of CYP3RNA-expressing plants show a slight peak of siRNAs reads matching to an approximately 100 nt long region in the 294 nts CYP51A fragment (Figure 1(e); Figure 2(e); Figure 3 (a)(b)). We assessed whether a dsRNA construct covering this region is sufficient to confer HIGS-mediated resistance to *Fg* in Arabidopsis. For this, transgenic Arabidopsis plants expressing the 100 nts region of the CYP51A fragment (named "Hotspot-A": positions 343 to 443 nt in CYP3RNA, see Figure 3 (a); Supplementary Figure 3) were analysed for *Fg* infection. We found that Hotspot-A plants exhibited a degree of resistance towards *Fg* infection comparable to CYP3RNA-expressing plants (Figure 3(c)(d)). Moreover, these plants induced high levels of *FgCYP51A* silencing and *FgCYP51B* co-silencing, while *FgCYP51C* expression was not silenced (Figure 3(e)). This observation is consistent with the recent finding that CYP51-dsRNA constructs that target one or two *FgCYP51* genes induce co-silencing [47]. However, co-silencing of *FgCYP51B* can be explained by off-target hits of siRNA-derived from Hotspot-A fragment whereas no off-targets were detected for *FgCYP51C* (Figure 3(f)).

ESCRT-III is required for HIGS-mediated *Fg* resistance

Since EVs isolated from transgenic CYP3RNA-expressing Arabidopsis plants contain CYP3RNA-derived siRNA, we predicted that the translocation of transgene-derived siRNA involves operational plant intraluminal vesicles (ILVs) and MVB-mediated release of EV at the plant-fungal interface [5]. To test this prediction, we first selected seven Arabidopsis T-DNA

KO mutants that are impaired in endosomal sorting complex required for transport III (ESCRT-III) to assess whether a transfer of CYP3RNA-derived siRNAs is compromised in plants with a defective exosomal vesicle pathway. The KO mutants were co-transformed with CYP3RNA and subsequently genotyped and propagated (Supplementary Table 3). The T2 generation of transgenic plants *Δvps2*-CYP3RNA, *Δvps20*-CYP3RNA, *Δrabf1*-CYP3RNA, *Δrabf2a*-CYP3RNA, *Δrabf2b*-CYP3RNA, *Δsnf7a*-CYP3RNA, *Δsnf7b*-CYP3RNA, and *Δsnf7c*-CYP3RNA were further investigated. Infection of detached leaves with *Fg* showed that virtually all tested CYP3RNA-generating ESCRT-III mutants were more susceptible to the fungus as compared with CYP3RNA-expressing non-mutated plants (Figure 4(a)), raising the possibility that a functional ESCRT-III is required for HIGS.

To substantiate this finding, we isolated EVs from the five mutant lines *Δvps20*-CYP3RNA, *Δvps2*-CYP3RNA, *Δsnf7a*-CYP3RNA, *Δsnf7b*-CYP3RNA, and *Δsnf7c*-CYP3RNA to analyse vesicle size distribution by TEM and NTA (Figure 4(b)(c)). *Δvps20* and *Δvps2* mutants are compromised in EV functionality as VPS20 (VACUOLAR PROTEIN SORTING-ASSOCIATED PROTEIN 20) is recruited by ESCRT-II to start the assembling of ESCRT-III, while VPS2 is needed for EV membrane invagination and the formation of EVs. The RAB (RAS-REALATED-PROTEIN) GTPases are key players in the regulatory process of endosomal vesicle transport. NTA revealed particle sizes between 100 nm and 150 nm with an average size (diameter) of 139 +/- 7.7 nm for wt plants, 115 +/- 9.9 nm for CYP3RNA-expressing plants, 133 +/- 11.6 nm for *Δvps2*-CYP3RNA, 139 +/- 7.7 nm for *Δvps20*-CYP3RNA (Figure 4(c)(d)). As expected, NTA displays slightly bigger particle sizes than EV size measurement by TEM. Accordingly, TEM analysis revealed EVs diameter of 101 nm (wt), 86 nm (*Δvps2*-CYP3RNA), and 107 nm (*Δvps20*-CYP3RNA) (Figure 4(c)(d)). To further investigate the morphology of EVs, we performed lipid and protein staining as well as sample fixing by uranyl acetate (UAc) and NanoW, prior analysing EVs by TEM (Figure 4(e)). When EVs were stained with UAc, PBS buffer in the EV suspension leads to poor background signals.

To obtain a better contrast we negatively stained EVs with NanoW. As expected, NanoW leads to less background signals and higher contrast (Figure 4(e)). EVs from wt Arabidopsis showed round shaped borders between intravesicle lumen and environment, with a heterogenous inside after staining with UAc and NanoW (Figure 4(e)). In contrast, EVs from *Δvps20*-CYP3RNA are also round shaped and have a smooth and clear boundary to the environment, but UAc staining reveals a homogenous inner structure (Figure 4(e)), while NanoW staining show similar heterogenous intravesicle structures like in wt EVs (Figure 4(e)). We have no explanation why both staining methods lead to such a different appearance. EVs of the *Δvps2*-CYP3RNA mutant instead have no clear shaped borders compared to wt and *Δvps20*-CYP3RNA plants independently of the staining agent (Figure 4(e)). The edges look very diffuse and rough while the inside has different and complex structures like EVs from the wt. Thus, loss of function mutations in both genes probably lead to aberrant EV structures and sizes which might contribute to the loss of EV-mediated siRNA transport. For *Δsnf7a*-CYP3RNA, *Δsnf7b*-CYP3RNA, and *Δsnf7c*-CYP3RNA we observed no differences among EVs isolated from *snf7* plants using NTA (Figure 4(c)). Important to note, subsequent TEM analysis revealed only one EV-like structure in isolated EV samples of *Δsnf7a*-CYP3RNA indicating that co-isolated extracellular particles or aggregates led to similar/indistinguishable NTA results, which are only stable in liquid environments and therefore not visible during TEM where samples are dehydrated during staining procedure.

EVs from dsRNA-sprayed barley leaves contain less CYP3RNA-derived siRNAs

Our previous work suggested difference in RNA transfer and uptake by *Fg* depending on whether dsRNA is delivered via transgene-expression (HIGS) or spray (SIGS) [12,25,48]. Present knowledge suggests that HIGS involves plant-mediated processing of transgene-derived dsRNA into siRNAs and transfer to / uptake by the fungus. In contrast, when sprayed onto leaves, dsRNA is only partly processed by the plant, while unprocessed dsRNA is

transported in plant vessels and eventually taken up by *Fg* [12,56]. We examined whether EVs contain dsRNA-derived siRNAs upon spraying dsRNA onto leaves. Since the SIGS setup to our experience is extremely inefficient in the *Fg* - Arabidopsis interaction, we conducted a spray experiment using detached barley leaves. Upon spraying upper parts of detached leaves with 20 ng μl^{-1} CYP3RNA or TE-buffer as control (semi-systemic design, see MM and [12]), apoplastic fluid was collected from lower (not directly sprayed) leaf parts after 2 days of spraying. Harvested leaf segments were vacuum-infiltrated with VIB and centrifuged in 30 ml syringes placed in a 50 ml falcon tube for 20 min at 1,000 x*g* at 4°C. Following the preparation as described above for Arabidopsis, the F48 fraction contained vesicles ranging from 100 nm to 200 nm in diameter with an average of 167 nm for the TE-buffer and 156 nm for the CYP3RNA-treated plants (Table 1; Supplementary Figure 6(a)), while the F100 fraction did not contain vesicles (Supplementary Figure 6(b)). The overall yield of EVs from 1 ml of apoplastic washing fluid was much lower than for Arabidopsis. Despite the low EV recovery, RNA extraction from the F40 fraction yielded a sufficient amount of RNA for cDNA library preparation and sequencing (Supplementary Table 2). EVs from CYP3RNA-sprayed samples contained siRNAs mapping to CYP3RNA (Supplementary Figure 6(c)). In general, the overall number of siRNAs that mapped to the CYP3RNA was lower compared to both Arabidopsis samples and also read coverage (number of reads that overlap at a certain position of the sequence) was low (Supplementary Figure 6(c)).

Comparative proteomic analysis of Arabidopsis EVs

To gain further insight into the protein content of EVs we conducted a proteomic comparative analysis of Arabidopsis EVs using our data and compared them to published data [27]. To this end, EVs were isolated from apoplastic washes of 5-wk-old Arabidopsis wt plants as described [27]. By categorizing the proteins to GO-terms we observed a 2-fold enrichment of proteins associated with stress responses and abiotic stimuli compared to the whole proteome as

previously described by Rutter and Innes [27] (Figure 5(a)(b)(c)). Moreover, we observed a 6-fold and 2-fold enrichment of proteins associated with translation and proteins of the categories transport and cellular component organization, respectively. Comparing the identified proteins by Rutter and Innes [27] with MS data of this study we found an overlap of 81 proteins identified in both studies (Figure 5(d)). Remarkably, these overlapping proteins are specifically proteins with high abundance in both studies and the 15 proteins with the highest abundance are identical. Following the procedure of Rutter and Innes [27] we further classified the identified proteins to GO-terms via the PANTHER Classification System (Supplementary Figure 7-9). However, we assume that differences in the protein profiles resulted from using plants of different age and divergent genotypes. For example, Rutter and Innes [27] isolated EVs from 5-7-wk-old, genetically modified (GFP-PEN1) Arabidopsis plants, while we used 4-5-wk-old wt Col-0 Arabidopsis plants.

Discussion

The discovery that plants have evolved the capability of silencing foreign transcripts trough RNAi by their own sRNAs [49] or after biotechnological manipulation by sRNA derived from a dsRNA-generating transgene is especially relevant for future agricultural applications. The latter possibility, called HIGS [57] has been used to successfully engineer resistance to a broad range of pests and microbial pathogens [22,58,59]. It is an exciting possibility that plant EVs mediate the interspecies transfer of RNAs in natural cross-kingdom communications [22,28]. Supporting this notion, we show here that EVs purified from leaf extracts and apoplastic fluids of transgenic Arabidopsis HIGS plants expressing long dsRNA contain dsRNA-derived siRNAs. This finding substantiates that EVs are key mediators in host-pathogens communication and shows for the first time that EVs carry sRNA cargo for silencing foreign transcripts in HIGS strategies.

Because fungi probably lack RNA transporters, such as SID1 and SID2 found in nematodes and insects, RNA uptake during plant-fungus communication via membrane-localized RNA transporters is an unlikely option. Thus, several recent reports suggest a bidirectional sRNA transport via EVs [22,28,60] in analogy to the role mammalian exosomes have in cell-to-cell communication [39,61-64]. In line with this knowledge, we followed the hypothesis that sRNA transfer in HIGS also is vesicle-based. As an essential basis, we used recently developed protocols [27,65] for the isolation of EVs and their cargo from Arabidopsis leaves. Vesicles isolated by these methods were around 140 nm (139 +/- 7.7 nm) in diameter (Figure 2), which is in good agreement with the size range reported for small EVs from mammalian cells (30-150 nm [66]) and plants (50-300 nm [27]). The physical appearance of vesicles in the TEM analysis was comparable to typical exosome preparations from cell culture supernatants [67], especially as they were surrounded by a characteristic lipid bilayer which has an average thickness of around 5 nm in diameter (Figure 1; Figure 2). Moreover, mammalian EVs have a density of 1,13-1,19 g/ml [68], which fits well with the detection of the Arabidopsis vesicles in the sucrose gradient between the 30% and 45% sucrose corresponding to a density of 1.1270 g/ml and 1.2025 g/ml, respectively. Vesicles isolated from Arabidopsis cell extracts showed a slightly more cup-shaped morphology than those from the apoplastic fluid. Cup-shaping of exosomes is an effect of extreme dehydration during conventional TEM procedures [27, 67]. This effect can be more or less severe during different sample preparations, thus explaining the different appearance of Arabidopsis vesicles.

Sucrose gradient centrifugation has been repeatedly used for mammalian EV purification and subsequent RNA sequencing. From our point of view, gradient centrifugation currently represents one of the most stringent method to obtain different EV subpopulations, according to their buoyant density [69,70]. As a precautionary measure, we treated vesicles with RNase A, an endoribonuclease that specifically degrades single-stranded RNA at C and U residues, to further remove potential contamination from outside adhering RNA. RNA-seq analysis of the

cargo of vesicles both from whole leaf extracts and apoplastic fluids contain sRNA. Moreover, using transgenic Arabidopsis expressing the dsRNA CYP3RNA we demonstrate that EVs carry transgene-derived siRNA cargo (Figure 2). Previous work showed that the 791 nt long CYP3RNA, when expressed in Arabidopsis or barley, inhibits the infection *Fg* by targeting the transcripts of its three *FgCYP51* genes via RNAi [12,47,71]. Together these findings support the view that HIGS includes processing of dsRNA in the plant, incorporation of the produced siRNA into intracellular vesicles, secretion of the vesicles into the apoplastic space, and a potential uptake of the vesicles or their cargo into the interacting fungus (Figure 6). This scenario is supported by several lines of evidences from earlier reports: Fungal and bacterial infection activated the biogenesis and enhanced the formation of vesicles between cell wall and cell membrane, and these vesicles contain defence related compounds [27,30,72]. Arabidopsis LIP5 (HOMOLOG OF MAMMALIAN LYST-INTERACTING PROTEIN5), a positive regulator of MVB biogenesis, is a critical target of pathogen-responsive MAPK cascade in plant basal defence [72]. MVBs and paramural bodies proliferate underneath papillae in barley cells during powdery mildew infection. MVBs were also observed in fungal haustoria and in association with plasmodesmata, suggesting that the secretion of EVs contributes to the formation of defensive appositions, but may also help block plasmodesmata in cells undergoing HR and contribute to defense-related endocytosis [29,43].

The PEN1 protein is secreted outside of the cell during powdery mildew infection and is encased in the papillae along with membranous material. The same is true for PEN3, SNAP33 (SOLUBLE N-ETHYLMALEIMIDE-SENSITIVE FACTOR ADAPTOR PROTEIN 33), and VAMP722 (VESICLE-ASSOCIATED MEMBRANE PROTEIN 722), suggesting that PEN1 is secreted inside vesicles (Figure 2(d)), like exosome secretion in mammals [73]. Finally, EVs isolated from the apoplastic fluids of sunflower (*Helianthus annuus*) contained families of proteins commonly found in mammalian and Arabidopsis EVs. EVs labeled with FM 4-64 were

taken up by *Sclerotinia sclerotiorum* spores, reduced hyphal growth and permeabilized fungal membranes, as evidenced by the uptake of otherwise non-permeable dyes [74].

sRNA cargo of EVs has been shown for fungi [60], nematodes [75] and plant pathogenic bacteria [76]. In mammalian cells, sRNAs of parasitic origin are transported to host cells via vesicles [77,78]. It remains unclear how specificity is achieved regarding which RNAs are packed into vesicles or how RNAs are selectively incorporated into different classes of EVs. Of note, we found that EVs from sprayed barley leaves contain less SIGS-derived sRNAs indicating different molecular mechanisms underlying the transgene-based (HIGS) or spray-mediated (SIGS) delivery strategy, either requiring the plant's or the fungal RNA silencing machinery. Whereas HIGS virtually is based on the plant's silencing machinery, the mechanism of gene silencing by exogenously delivered dsRNA probably constitutes a more complex situation. For instance, our previous results point in the direction that the molecular mechanism of SIGS is controlled by the fungal silencing machinery [12]. In summary, our findings support the model that SIGS involves: *i.* uptake of sprayed dsRNA by the plant (via stomata, [12]); *ii.* transfer of apoplastic dsRNAs into the symplast by a yet unknown mechanism; *iii.* systemic translocation of siRNA or unprocessed dsRNA via the vascular system (phloem/xylem, [12,56]); *iv.* uptake of apoplastic dsRNA or symplastic dsRNA/siRNA by the fungus [12]; *v.* processing into siRNA by fungal DCLs [12]. Contrasting, the integration of our findings support the view that HIGS involves: *i.* processing of transgene-derived dsRNA in the plant ([12], unpublished data); *ii.* incorporation of the produced siRNA into intracellular vesicles (MVBs, Figure 6); *iii.* secretion of the vesicles (EVs) into the apoplastic space and uptake of the vesicles or their cargo into the interacting fungus (Figure 6). Supporting the notion that MVBs are involved in host-pathogen communication via their sRNA cargos, our results indicate that the ESCRT-III is required for HIGS-mediated *Fg* disease resistance as we demonstrated that KO mutants of ESCRT-III lost their resistance towards *Fg* infection. To further verify our results, we isolated EVs of two KO mutants Δ*vps2*-CYP3RNA and Δ*vps20*-

CYP3RNA. Notably, both mutants produced and released EVs which can be purified from apoplastic washes (Figure 4). We systematically measured diameters of wt Arabidopsis plants in comparison to both mutant lines, using NTA- and TEM-based analysis (Figures 4). Despite a slight size difference of Δ*vps2*-CYP3RNA, surface appearance and composition of both tested mutant lines were impaired supporting the importance of ESCRT-III components in CYP3RNA-mediated *Fg* resistance. VPS20 function as linker between ESCRT-I or ESCRT-II to ESCRT-III [79]. Therefore, we anticipate that *vps20* mutants were impaired in correct protein/RNA packaging into EVs leading to the release of CYP3RNA-free EVs. VPS2 is recruited by SNF7 and forms oligomers which leads to sculpting the MVB membrane for forming a dome which then forms an EV [79]. As Δ*vps2*-CYP3RNA releases smaller EVs, VPS2 somehow helps to stabilize and extend this membrane dome to form bigger EVs. Of note, consistent with our data, [22] demonstrated that MVBs fused to the plasma membrane releasing EV-packaged plant sRNAs at fungal infection sites to silence virulence genes in *Botrytis cinerea* thus suppressing fungal pathogenicity [22].

Profiling of CYP3RNA-derived siRNAs of HIGS Arabidopsis plants (Figure 3(a)) or fungal cell cultures treated with CYP3RNA [12] revealed a unique pattern where siRNAs that originate from the *FgCYP51A* fragment were overrepresented. Based on this finding we generated a HIGS construct covering the 100 nt peak-region of the *FgCYP51A* fragment. Remarkably, we found that those transgenic plants exhibited *Fg* disease resistance phenotypes comparable to the CYP3RNA-expressing plants (Figure 3(d)). Our results provide an example for successful *Fg* disease resistance that is mediated by a short 100 nt dsRNA construct. Interestingly, we detected only low numbers of siRNAs in EVs matching to *FgCYP51B* (Figure 2(e)). Such a minor transport of *FgCYP51B* targeting siRNAs to the fungus would strengthen the above discussed argument that the efficiency of the CYP3RNA is eminently boosted by co-silencing effects [72]. Another explanation for the silencing effects on *FgCYP51B* is probably the formation and amplification of secondary siRNAs in the fungus that provoke the target gene

silencing without an efficient generation and/or transport of *FgCYP51B* targeting siRNAs. Again, it is noteworthy that the library size was probably not sufficient to cover the whole range of vesicle contained siRNAs.

While we found strong indication for vesicle-mediated transport during RNAi-based plant protection approaches, many questions remain open: *i.* how are sRNAs packed into EVs; *ii.* what is the role of RNA-binding proteins in EV-packaging; *iii.* how can these vesicles cross the plant-fungus interface and *iv.* how are they released into fungal cells,. Here we provided significant insights into RNA uptake, processing and transport that is a step forward in unrevealing the mechanistic basis of HIGS as well as SIGS. However, further research is required to enhance efficacy and specificity of RNA-based plant protection for making them a realistic and sustainable approach in agriculture.

Material and Methods

Plant infection assays

Fusarium graminearum (*Fg*) strain *Fg*-IFA65 (IFA, Department of Agrobiotechnology, Tulln, Austria was cultured on synthetic nutrient-poor agar (SNA)-medium [59]. Plates were incubated at room temperature (RT) under constant illumination from one near-UV tube (Phillips TLD 36 W/08) and one white-light tube (Phillips TLD 36 W/830HF). For all leaf inoculation assays, *Fg* conidia suspensions were adjusted to 5×10^4 conidia per ml^{-1} [12]. *Arabidopsis thaliana* Col-0 wild type (wt) and transgenic plants were grown in a climate chamber under short day conditions with 8 h light at 22°C with 60% relative humidity. For infection, twenty rosette leaves of 15 5-wk-old Arabidopsis plants were detached and transferred in square Petri plates containing 1% water agar. Detached leaves were wound inoculated as described [12]. Lesion size (in millimeters) was recorded 3 days post inoculation (dpi) from the digital images using the free software ImageJ program (http://rsb.info.nih.gov/ij/index.html). The percentage of leaf area showing water-soaked spots

with chlorotic and/or necrotic lesions (symptoms of a successful *Fg* infection; [12]) relative to the non-inoculated leaf was calculated.

Generation of transgenic Arabidopsis plants

The ESCRT-III knock-out (KO) mutants NASC ID: *vps2*-N661671, *vps20*-N669857, *snf7a*-N547108, *snf7b*-N676240, *snf7c*-N674613, *rabf1*-N658064, *rabf2a*-N512028, *rabf2b*-N656748 were obtained from Nottingham Arabidopsis Stock Centre (NASC) (Supplementary Table 3) and transformed to express CYP3RNA (as described in [12]) in ESCRT-III KO background resulting in the following transgenic lines: Δ*vps2*-CYP3RNA, Δ*vps20*-CYP3RNA, Δ*snf7a*-CYP3RNA, Δ*snf7b*-CYP3RNA, Δ*snf7c*-CYP3RNA, Δ*rabf1*-CYP3RNA, Δ*rabf2a*-CYP3RNA and Δ*rabf2b*-CYP3RNA. For generation of Arabidopsis Hotspot-A plants fungal *FgCYP51* gene sequence information was obtained from the database of the Broad Institute (www.broadinstitute.org). Primers were designed to generate PCR amplicon of 100-bp length corresponding to the exon of the selected gene *CYP51A* (FGSG_04092; Supplementary Figure 3(a)). Genomic template DNA was extracted from *Fg* using DNeasy Plant Mini Kit (Qiagen). Constructs for plant transformation were obtained by inserting the corresponding CYP51A-derived sequence between the *Hind*III and *Xma*I restriction sites of p7U10 RNAi (DNA cloning service). The plasmids were introduced into *Agrobacterium tumefaciens* strain AGL1 [80] by electroporation. Transformation of Arabidopsis was performed as described [81] and transgenic plants were selected on 1/2 x MS (Murashige and Skoog) agar plates containing 7 µg ml^{-1} BASTA (Duchefa). The transgenic lines for pathogen assays were selected based on transgene expression levels measured by qRT-PCR.

Isolation of vesicles from Arabidopsis leaves

For the isolation of vesicles, a published protocol was adjusted [65]. Ten 4-5-wk-old Arabidopsis rosette leaves were harvested and ground with pestle and mortar in a small amount

of 1x PBS buffer (140 mM NaCl, 2.5 mM KCl, 10 mM Na_2HPO_4, 2 mM KH_2PO_4, pH 7.4). The cell extract was collected on ice and larger particles were separated by sequentially centrifuged at 1,000 x*g* for 10 min (Eppendorf 5810R), 3,000 x*g* for 20 min, and 10,000 x*g* for 40 min at 4°C (Beckmann J2-21M/E). After the last centrifugation step, the supernatant was centrifuged at 160,000 x*g* for 90 min in an ultracentrifuge (Beckmann SW 41 Ti). The pellet was resuspended in 1 ml 1x PBS, loaded on top of a sucrose discontinuous gradient (8% / 15% / 30% / 45% / 60% w/v in 20 mM HEPES, pH 7.3), and centrifuged at 160,000 x*g* for 2 h. The bands between the 30% / 45% and the 45% / 60% sucrose layer were harvested separately. The respective fraction was filled up to 10 ml with 1x PBS and centrifuged again for 2 h at 160,000 x*g*. The pelleted vesicles were resuspended in a small amount of 1x PBS and analysed by TEM or subjected to RNA extraction and RNA sequencing.

Isolation of EVs from apoplastic washes of Arabidopsis leaves

A published protocol was adjusted to isolate EVs from Arabidopsis leaves [27]. Briefly, 5-wk-old rosette leaves were harvested, and vacuum infiltrated with vesicle isolation buffer (VIB: 20 mM MES, 2 mM $CaCl_2$ and 0.1 M NaCl, pH 6) until infiltration sites were visible. The infiltrated leaves were drained carefully on filter paper and centrifuged (Eppendorf 5810R) in 30 ml syringes placed in 50 ml falcon tubes for 20 min at 700 *g* and 4°C. The resulting apoplastic fluid was filtered through 0.45 µm sterile filters, followed by centrifugation at 10,000 *g* for 30 min at 4°C (Eppendorf 5417R). The supernatant was then diluted to 10 ml with VIB and centrifuged for 1 h at 48,000 *g* at 4°C (Beckmann J2-21M/E). The resulting pellet was washed with 10 ml PBS and finally resuspended in a small amount of PBS (fraction $EV_{apo\text{-}Ath}$). For further analysis samples were stored at 4°C for a maximum of two days.

Isolation of EVs from CYP3RNA-sprayed barley leaves

Barley cv. Golden Promise plants were grown under 16 h light (Osram Lumilux® Cool White L 30W/840, Osram L 36W/77 FLUORA G13, relation 4:2) at 22°C with 60% relative humidity. Ten detached second leaves of 3-wk-old plants were transferred in square Petri dishes containing 1% water agar. For spray application, the 791 nt dsRNA CYP3RNA (Supplementary Figure 3(b); [12]) was generated using the MEGAscript RNAi Kit (Invitrogen) following the manufacturer's instructions. CYP3RNA eluted in TE-buffer (10 mM Tris-HCl pH 8.0, 1 mM EDTA) was diluted with water to a final concentration of 20 ng μl^{-1}. For control, TE-buffer (without CYP3RNA) was diluted with the same amount of water. Upper leaf parts of detached leaf segments were sprayed with 500 µl of 20 ng μl^{-1} CYP3RNA/TE-buffer solution or TE-buffer and incubated at RT as described [12]. After 48 h, unsprayed lower leaf parts were harvested, washed for 5 min in H_2O and vacuum infiltrated with VIB until infiltration sites were visible as dark green areas. Infiltrated leaves were drained and centrifuged in 30 ml syringes placed in a 50 ml falcon tube for 20 min at 1,000 *g* at 4°C. The next steps were done as described above for Arabidopsis apoplastic fluids resulting in the fraction $EV_{apo\text{-}barley}$.

RNA extraction for RNA sequencing

Before RNA isolation, vesicles of the fractions $EV_{apo\text{-}Ath}$ and $EV_{apo\text{-}barley}$ were treated with RNase (0.4 ng μl^{-1} RNase A; Thermo Fisher Scientific) to remove extravesicular RNA. Samples were incubated for 10 min at 37°C and then kept on ice. Vesicle RNA was isolated using the Single Cell RNA Purification Kit (Norgen Biotek) according to the manufacturer's instructions described for cells growing in suspension. RNA concentrations were determined using the NanoDrop spectrophotometer (Thermo Fisher Scientific) and RNA was stored at -80°C.

Small RNA sequencing and bioinformatics analysis

Indexed sRNA libraries were constructed from RNA isolated from vesicles with the TruSeq® Small RNA Library Prep Kit (Illumina) according to the manufacturer's instructions. Indexed sRNA libraries were pooled and sequenced on the Illumina MiSeq Platform (1 x 36 SE) and the sequences were sorted into individual datasets based on the unique indices of each sRNA library. The quality of the datasets was examined with fastqc before and after trimming. The adapters were trimmed using cutadapt [82] version 1.14. The trimmed reads were mapped to the CYP3RNA sequence using bowtie2 [83] version 2.3.2. to identify siRNAs derived from the precursor dsRNA sequence. The mappings were first converted into bedgraph using bedtools [84] version 2.26.0 and then to bigwig using bedGraphToBigWig [85]. These files were used for visualization with IGV [86]. Read coverage is defined as the number of reads that match at a certain position of the sequence.

Negative staining and transmission electron microscopy (TEM)

For TEM, copper formvar-coated 300-mesh electron microscopy grids were glow discharged prior to sample application for 40 sec. Subsequently, 5 µl of $EV_{apo\text{-}barley}$ and all $EV_{apo\text{-}Ath}$ genotypes resuspended in PBS were applied to the grids. Samples were dabbed off using Whatman filter paper and grids were washed three times in 50 µl of 2% uranyl acetate. Additionally, protein and lipid staining were performed. 55 µl vesicles were incubated for 3 min with 0.1% solution of glutaraldehyde and 3% paraformaldehyde for protein staining. Afterwards, vesicles were washed with PBS before samples were incubated with 1% osmiumtetraoxide solution for 1 min for lipid staining, followed by a second washing step with PBS. All dyes were diluted in PBS before staining. Finally, samples were negative stained and fixed with 2% uranyl acetate or NanoW, an organotungsten based negative staining agent, as described before and washed with water. Needless staining or fixing solutions, buffers and water were removed by Whatman paper between each step. Finally, grids were air dried.

Preparations were inspected at 120 kV under zero-loss conditions (ZEISS EM912a/b) and images were recorded at slight underfocus using a cooled 2k x 2k slow-scan ccd camera (SharpEye / TRS) and the iTEM software package (Olympus-SIS).

Vesicle size and concentration measurements by nanoparticle trafficking analysis (NTA)

For size and concentration prediction, purified EVs of *Arabidopsis thaliana* (wt), Δ*vps2*-CYP3RNA, Δ*vps20*-CYP3RNA, *Δsnf7a*-CYP3RNA, *Δsnf7b*-CYP3RNA, and *Δsnf7c*-CYP3RNA were diluted (1:50) with PBS. Subsequently, 500 µL of vesicle suspension was loaded into Nanosight NS300 (Malvern Panalytical). 5 measurements were performed at 25°C and size, concentration prediction and statistical analysis were performed by the NTA 3.2 Dev Build 3.2.16 software.

PEN1 detection by immunoblot analysis

EVs were treated by 1% Triton100 water solution (Sigma-Aldrich), 4 µl of 10 µg ml^{-1} trypsin in 10 mM HCl or both beside an untreated control [27]. Protein of whole cell extract and of EVs were separated by electrophoresis and blotted onto a nitrocellulose membrane. The membrane was blocked by 5% milk powder in Tris buffered saline (TBS; 100 mM Tris, 150 mM NaCl) containing 0.1 % Tween at 4°C over night. After blocking the membrane was incubated with an anti-PEN1 antibody [27] 1:5000 for 4 h at RT. A secondary antibody (Thermo Fisher Scientific) linked to horseradish peroxidase was diluted 1:10000 in TBS and used for one hour at RT before detection by chemiluminescence using Amersham™ ECL™ Prime Western Blotting Detection Reagent (GE Healthcare) following manufactures instructions.

In-solution tryptic digestion

Pellets of isolated EV fractions were washed twice with 50 mM ammonium bicarbonate buffer using Amicon Ultra 3 kDa cut-off centrifugal filters (Merck Millipore Ltd), and total protein

concentration was estimated using Quick Start Bradford Protein Assay (Bio-Rad Laboratories). Protein samples were subjected to in-solution tryptic digestion followed by mass spectrometry (MS) analysis as described earlier with minor modifications [87]. In brief, proteins (20 µg) were diluted with 50 mM ammonium bicarbonate buffer containing 0.1% RapiGest (Waters), followed by incubation at 80°C for 15 min. The denatured proteins were then reduced with 100 mM dithiothreitol for 15 min at 65°C, and alkylated with 200 mM iodoacetamide at room temperature in the dark for 30 min. Sequencing grade modified trypsin (Promega Corporation) was added in 1:20 ratio (trypsin/protein, w/w) and the mixture was incubated overnight (16 h) at 37°C. Tryptic digestion reaction was stopped by adding 2 µl of concentrated formic acid and incubated for 10 min at 37°C before being centrifuged. Digested peptides were desalted using C_{18} zip tips (Millipore) and concentrated using vacuum concentrator. Dried peptides were reconstituted in aqueous 3% acetonitrile with 0.1% formic acid.

Proteomic analysis

Peptide digests (2 µg) were separated by using a Dionex Ultimate 3000 UHPLC system (Thermo Fisher Scientific) equipped with a reversed-phase Kinetex C18 2.6 µm column (100 X 2.1 mm, 100 A°). The sample was loaded onto the column with 97% of mobile phase A (100% water with 0.1% formic acid) and 3% mobile phase B (100% acetonitrile with 0.1% formic acid) at 250 µl/min flow rate. Peptides were eluted with a 120 min linear gradient of 3 to 50% of mobile phase B. The column and autosampler compartments were marinated at 40°C and 4°C respectively. Proteomic datasets were acquired in a data-dependent ($ddMS^2$-top 10) manner using a hybrid quadruple orbital trapping mass spectrometer (Q Exactive; Thermo Fisher Scientific) in positive-ion mode as described earlier [88]. MS data files (of three biological replicates) were processed using Proteome Discoverer software (version 2.2.0.388, Thermo Fisher Scientific) with Sequest HT search algorithm. The raw data were searched against UniProt Arabidopsis protein database (reviewed, downloaded on 19th June 2018).

Search parameters included trypsin as proteolytic enzyme with two missed cleavages and 1% false discovery rate. Peptide precursor and fragment mass tolerance were set to 10 ppm and 0.6 Da, respectively. Search criteria also included carbamidomethylation (C) as fixed modification, protein N-terminal acetylation and oxidation (M) as variable modifications. As regulated, only proteins with a minimum of two peptides were considered for further analysis. Identified proteins were categorized according to molecular functions, biological processes, and cellular components based on gene ontology (GO) annotations using "The Arabidopsis Information Resource" (https://www.arabidopsis.org/tools/bulk/go/index.jsp).

Acknowledgements

We thank C. Birkenstock, U. Schnepp and V. Weisel for excellent plant cultivation and M.Sc. C. Pfafenrot and M.Sc. M. Mosbach for helping with the NTA measurements. We thank Roger Innes for providing us the PEN1 antibody. We thank the Salk Institute Genomic Analysis Laboratory for providing the sequence-indexed Arabidopsis T-DNA insertion mutants. This work was supported by the Deutsche Forschungsgemeinschaft, Research Training Group (RTG) 2355 (project number 325443116) to KHK and AK. VG thanks the German Academic Exchange Service (DAAD) for a doctoral fellowship. Financial support by the Deutsche Forschungsgemeinschaft (Sp 314/13-1 and INST 162/500-1 FUGG) is gratefully acknowledged.

Competing financial interests

The authors declare no competing financial interests. Work on Fusarium CYP3RNA (Koch et al. 2013) is subject of a patent application (WO2015004174A1).

Author Contributions

K-H.K., A.K. and L.H. wrote the manuscript; A.K. and K-H.K designed the study; T.S., L.H., D.B., V.G., C.P., and M.C. conducted the experiments; K-H.K., A.K., T.S., L.H., V.G., B.S. and B.W. analyzed all data and drafted the figures. L.H. and T.B. conducted RNA-seq experiments and B.W., T.B., J.K., and L.J. performed bioinformatics analysis. All authors reviewed the final manuscript.

Legends to Figures

Figure 1. **Vesicle isolation from Arabidopsis whole leaf cell extracts purified by sucrose-gradient centrifugation.** (a)(b) Vesicles from wt Col-0 (a) and CYP3RNA-expressing (b) plants were subjected to sucrose gradient centrifugation at 160,000 *g* resulting in two predominant greenish bands between the 30% - 45% (upper band, F160-s1) and 45% - 60% (lower band, F160-s2). Vesicles were analysed by negative staining and TEM. The fraction F160-s1 contained vesicles with a size range of 50-200 nm. Most of them were cup-shaped and surrounded by a layer reminiscent of a membrane. (c) Profiling of CYP3RNA-derived siRNAs by sRNA-seq. Total RNAs were isolated from vesicles of fraction F160-s1 of the sucrose gradient containing vesicles with average sizes of 95 nm and 105 nm (see Table 1). sRNA reads of max. 25 nt from CYP3RNA-expressing (CYP3RNA-HIGS) and wt plants were mapped to CYP3RNA that represents sequences of the *FgCYP51A*, *FgCYP51B* and *FgCYP51* C gene of *Fg* [12,25]. Sequencing data are gained from two pooled separate vesicle isolations experiments. (d) sRNA profiling of vesicles isolated from leaf cell extracts of CYP3RNA-expressing Arabidopsis plants. There is a bias of siRNA reads mapping to the CYP3RNA sequence as most reads map to the *FgCYP51A* fragment of the precursor. (e) Size distribution of total RNA-reads isolated from wt plants, CYP3RNA plants and reads matching to the CYP3RNA precursor.

Figure 2. **Analysis of EVs from the apoplastic fluid of Arabidopsis leaves.** (a)(b) Negative staining and TEM of pellets of the 48,000 *g* (fraction F48, (a) i-iii) and the 100,000 *g* (F100, (b)) centrifugation. Pictures are shown exemplary for CYP3RNA-expressing (a) (i,ii) and wt plants (a) (iii) (b). Experiments were performed multiple times with similar results. (c) Size measurements by nanoparticle trafficking analysis (NTA) Particle concentration per particle size per measurement. Averaged particle concentration per particle size purified from apoplastic washes of Arabidopsis CYP3RNA plants (black line) and +/- 1 standard error (red). Purified EVs have an average size of 139 +/- 7.7 nm the sample concentration was 1.0×10^{10} +/- 5.2×10^{8} particles/ml. (d) PEN1 detection was performed by western blot analysis. Therefore, protein of whole cell extract (lysate) and of isolated EVs were separated by electrophoresis and blotted on to a nitrocellulose membrane. Before separating, EVs were treated by Triton100, trypsin or both beside an untreated negative control. PEN1 were detected in all lanes, but signal intensity is dramatically reduced after EVs were treated by Triton100 and trypsin while treatment by only Triton100 or trypsin leads to no signal intensity. (e) Profiling of CYP3RNA-derived siRNAs in EVs from the apoplastic fluids of Arabidopsis leaves. Vesicles were isolated by apoplastic washes. Total RNA extraction was performed from purified vesicles and analysed by sRNA-seq. sRNA reads of max. 25 nt from CYP3RNA-expressing (CYP3RNA-HIGS) and wt plants are mapped to the sequence of the CYP3RNA that represents sequences of the *FgCYP51A*, *FgCYP51B* and *FgCYP51* C gene of *Fg* [12]. Sequencing data are gained from vesicle isolation from the apoplastic fluid of each 10 CYP3RNA-expressing or wt plants. (f) Read length distribution of sRNAs isolated from apoplastic washes of wt plants (i), CYP3RNA plants (ii), and reads of CYP3RNA plants with perfect complementarity to the CYP3RNA precursor (iii). (g) Nucleotide distribution of unique 21 nt sRNAs isolated from apoplastic washes of wt plants (i), CYP3RNA plants (ii), and reads of CYP3RNA plants with perfect complementarity to the CYP3RNA precursor (iii).

Figure 3. **HIGS in *Fg* upon infection of transgenic Arabidopsis expressing 100 nt Hotspot-A-dsRNA.** (a)(b) sRNA profiling of leaf cell extracts isolated from CYP3RNA-expressing Arabidopsis plants (a). There is a bias of siRNA reads mapping to the CYP3RNA sequence as most reads map to the *FgCYP51A* fragment of the precursor (b). (c)(d)(e) HIGS-mediated inhibition of *Fg* infection on Arabidopsis leaves expressing 100 nt Hotspot-A-dsRNA. (c) Fifteen detached rosette leaves of Hotspot-A-expressing Arabidopsis plants (T2 generation) were drop-inoculated with 5 x 10^4 conidia ml^{-1}. Infection symptoms were evaluated at 5 dpi. (d) Quantification of the visibly infected area at 5 dpi shown as percent of the total leaf area. Error bars represent SE of three independent experiments, each using 15 leaves of 10 different plants for each transgenic line. Asterisks indicate statistical significance (**p<0,01; ***p<0,001; students t-test). (e) Gene-specific expression of *FgCYP51A*, *FgCYP51B*, and *FgCYP51C* was measured by qRT-PCR. Gene expression was first normalized against the fungal reference gene *EF1-α* (FGSG_08811) and subsequently normalized against the Δ-ct of the respective control. cDNA was generated after total RNA extraction from infected leaves at 5 dpi. The reduction in *FgCYP51* gene expression in the *Fg*-inoculated dsRNA-expressing leaves compared to the wt control was statistically significant. Error bars represent SE of three independent experiments each using 15 leaves of 10 different plants for each transgenic line. Asterisks indicate statistical significance (*p<0,05; **p<0,01; ***p<0,001; students t-test). (f) Potential targets of CYP3RNA-derived 21 nt sRNAs in the three *FgCYP51* genes. All possible CYP3RNA-derived 21mers were targeted against each *FgCYP51* gene with the plant miRNA target prediction algorithm TAPIR. The number of sRNAs targeting each region is plotted to the y-axis and the respective position of the gene is plotted to the x-axis. Each RNAi trigger sequence is plotted in the respective colour (CYP51A in red, Hotspot-A in green, CYP51B in blue and CYP51C in purple).

Figure 4. **Analysis of ESCRT-III KO mutants in HIGS-mediated *Fg* resistance.** (a) HIGS in *Fg* upon infection of transgenic Arabidopsis expressing CYP3RNA in ESCRT-III knock-out mutant background. Fifteen detached rosette leaves of CYP51-dsRNA-expressing Arabidopsis plants (T2 generation) were drop-inoculated with 5 x 10^4 conidia ml^{-1}. Infection symptoms were quantified of the visibly infected area at 5 dpi shown as relative infected leaf area. The average relative infected leaf area was normalized against Col-0 control plants and a total of 3 to 6 repetitions were conducted, each using 15 leaves of 10 different plants for each transgenic line. Each dot represents one repetition and the underlying box and whisker plots represent the median and quartiles of said repetitions. Asterisks indicate statistical significance (**p<0,01; ***p<0,001; students t-test; two-sided). (b) EVs of wt, *Δvps20*-CYP3RNA, *Δvps2*-CYP3RNA, *Δsnf7a*-CYP3RNA, *Δsnf7b*-CYP3RNA, and *Δsnf7c*-CYP3RNA were isolated by apoplastic washes and prepared for TEM analysis by negative staining with UAc and NanoW. EVs or the single EV like structure of *Δsnf7a*-CYP3RNA were marked by red arrows. (c) Particle size measurements by NTA analysis of particles isolated by apoplastic washes from Arabidopsis wt, *Δvps20*-CYP3RNA, *Δvps2*-CYP3RNA, *Δsnf7a*-CYP3RNA, *Δsnf7b*-CYP3RNA, and *Δsnf7c*-CYP3RNA. (d) Mean and mode values of the particle diameter from Arabidopsis wt, *Δvps20*-CYP3RNA, *Δvps2*-CYP3RNA, *Δsnf7a*-CYP3RNA, *Δsnf7b*-CYP3RNA, and *Δsnf7c*-CYP3RNA isolated apoplastic particles. Diameters were calculated by the NTA 3.2 Dev Build 3.2.16 software for the NTA measurements seen in (c). (e) EVs were purified by apoplastic washes from Arabidopsis wt plants and Δ*vps2*-CYP3RNA and Δ*vps20*-CYP3RNA mutants. EVs were resuspended in PBS and afterwards stained with glutaraldehyde, formaldehyde and osmium tetraoxide before negative staining was performed by using 2 % uranyl acetate (UAc) and NanoW.

Figure 5. **Functional categorization of EV-contained proteins.** PSMs for UniprotKB accessions were linked to Arabidopsis genes with the R package biomaRt. UniprotKB accessions were searched in the athaliana_eg_gene dataset on plants.ensembl.org and linked to the corresponding ensembl_gene_id. These gene_ids were linked to Gene Ontology terms of the category biological processes. (a)(b)(c) The relative amount [%] of the 15 most abundant terms is shown for EV-contained proteins (a) compared to the whole proteome (b) with specific numbers and categories (c). (d) Venn-diagram comparing proteins found in EVs by Rutter and Innes [27] compared to the data obtained within this study. To accommodate for the higher number of PSMs in the later datasets only genes with at least 1‰ of total PSMs in the respective study were considered.

Figure 6. **Vesicle-mediated transfer of HIGS-derived RNAs**. A hypothetical siRNA translocation pathway involves the integration of a HIGS construct, its transcription into dsRNA and the translocation into the cytoplasm, where it is loaded and processed by DCL enzymes (yellow). The resulting siRNA duplexes are either delivered to the plant's RNA silencing machinery or are incorporated as duplexes into intraluminal vesicles (ILVs) that originate either from the Golgi body via the trans-Golgi network or from endocytosis at the cell membrane, respectively (circles light blue). The ILVs, consisting of several cargos, are internalized by MVBs that enter the secretory pathway (circles dark grey). MVBs fuse to the PPM followed by subsequent release of ILVs (now called exosomes) (circles light blue). Exosomes cross the cellular interface, entering the fungal cell and release their cargo, possibly including plants siRNAs (process unknown). The siRNAs may subsequently enter the fungal RNAi machinery resulting in target gene silencing where they are wrenched by the AGO protein QDE-2 (quelling deficient-2), while the passenger strand is removed by the exonuclease QIP (hexagon green). The guide strand remains in the RNA-induced silencing complex (RISC)

which is activated and targets complementary mRNAs, resulting in degradation and *CYP51* gene silencing, respectively.

Supplementary figures

Supplementary Figure 1. TEM analysis of fraction F160-s2 (a) and the interphase fraction (b) between the visible bands corresponding to F160-s1 and F160-s2 of the sucrose gradient shown in Figure 1(a). Material was prepared from CYP3RNA-expressing Arabidopsis rosette leaves.

Supplementary Figure 2. sRNA-seq Col-0 (sucrose gradient). sRNA profiling of EVs isolated from leaf cell extracts from CYP3RNA-expressing (CYP3RNA-whole leaves) and wt (wt-whole leaves) Arabidopsis plants. Tracks show the read coverage of sRNAs on the CYP3RNA construct (logarithmic scale, 0-10 reads). There are no reads matching the CYP3RNA in wt plants.

Supplementary Figure 3. NTA size distribution of particles isolated by apoplastic washes from Arabidopsis wt plants.

Supplementary Figure 4. sRNA-seq Col-0 (EVs). sRNA profiling of apoplastic EVs isolated from CYP3RNA-expressing (CYP3RNA-apoplast) and wt (wt-apoplast) Arabidopsis plants. Tracks show the read coverage of sRNAs on the CYP3RNA construct (logarithmic scale, 0-10 reads). There are no reads matching the CYP3RNA in wt plants.

Supplementary Figure 5. DNA sequence of the dsRNA Hotspot-A (a) and CYP3RNA (CYP51A in yellow, CYP51B in blue and CYP51C in green) (b).

Supplementary Figure 6. EVs from the apoplastic fluid of CYP3RNA sprayed barley leaves. Shown are negative staining and TEM of pellets after centrifugation at 48,000 xg (F40, A) and 100,000 xg (F100, B). Pictures are shown for CYP3RNA-sprayed (a)(i,ii) and TE-buffer-treated (a)(iii)(b) leaves. Experiments were performed multiple times with similar results.

Supplementary Figure 7. Bioinformatics analysis (Functional categorization based on GO annotation) of the Arabidopsis Col-0 EV proteome dataset depicting the biological processes involved by the proteins.

Supplementary Figure 8. Bioinformatics analysis (Functional categorization based on GO annotation) of the Arabidopsis Col-0 EV proteome dataset depicting the cellular components of the proteins.

Supplementary Figure 9. Bioinformatics analysis (Functional categorization based on GO annotation) of the Arabidopsis Col-0 EV proteome dataset depicting the molecular functions of the proteins.

Table 1 Average diameter of vesicles from Arabidopsis and barley.

Plant	Vesicle diameter [nm]	Source
Arabidopsis wt	94.8 (± 2.5)	whole leaves
Arabidopsis CYP3	105.2 (± 3.6)	whole leaves
Arabidopsis wt	118.6 (± 6.5)	apoplastic washes
Arabidopsis CYP3	141.4 (± 8.0)	apoplastic washes
barley TE	166.6 (±17.8)	apoplastic washes
barley CYP3	155.8 (±21.0)	apoplastic washes

Average diameter was analysed with the ImageJ Software based on microscopy scale bars. Standard errors (SE) are given in parentheses. Arabidopsis CYP3, CYP3RNA-expressing plants; barley TE / CYP3, barley sprayed with TRIS-EDTA buffer (TE) or 20 ng ul^{-1} CYP3RNA in TE.

Supplementary Table 1 Amount of RNA isolated from different vesicle preparations used for cDNA library preparation and subsequent RNA sequencing.

Vesicle source	RNA amount [ng]
At-CYP3, whole leaves	720
At-wt, whole leaves	1080
At-CYP3, apoplast	90
At-wt, apoplast	30
Hv CYP3	70
Hv TE	120

At-CYP3: CYP3RNA-expressing Arabidopsis, wt: wild type, Hv CYP3: barley sprayed with CYP3RNA, Hv TE: barley sprayed with Tris-EDTA-Buffer (Mock).

Supplementary Table 2 Number of reads (million) in datasets from sRNA sequencing of plant vesicle sRNAs.

Vesicle source	No. of reads	No. of reads after trimming
At-CYP3, whole leaves	5.7	5.3
At-wt, whole leaves	2.3	2.1
At-CYP3, apoplast	5.4	2.4
At-wt apoplast	2.9	0.7
Hv CYP3	2.8	2.6
Hv TE	2.8	2.6

Read number in million is shown before and after adapter trimming. Vesicles from CYP3RNA-expressing Arabidopsis (*At*) leaves and form barley (*Hv*) leaves sprayed with TRIS-EDTA buffer (TE) or 20 ng μl^{-1} CYP3RNA in TE.

Supplementary Table 3 List of primers used for genotyping of ESCRT-III KO mutants

target	SALK-ID/NASC	Primer pair
vps2	SALK_018194C	VPS2_LP TTTTCGACAAAATCTCAACCTG VPS2_RP ACGAAATCGAGAGAAAGGAGG
vps20	SALK_078060C	VPS20_LP AGTGTGGATGAAATCAAACCG VPS20_RP GAGCTCAGAACAAACTGTGCC
snf7a	SALK_047108	SNF7a_LP AAGCAAACACTCTGCACCATC SNF7a_RP CTCAGACCAAATTCGAGCAAG
snf7b	SALK_094142C	SNF7b_LP TGGAGGTAGATACAGGGAACCC SNF7b_RP TCATGATTTTGCTCCCACTTC
snf7c	SALK_040393C	SNF7c_LP AAACAGCCCAAGAAAGTATGC SNF7c_RP CACACTGCAACAATAAAGCCC
rabf1	SALK_004698C	RABF1_LP TTTCTCCTCGAACAAACGTTG RABF1_RP ATTACACCTTCGGAAAATGGG
rabf2a	SALK_012028	RABF2a_LP ACCGCAACAAATGTCAAAGAC RABF2a_RP AACAGGTTTGGAAGACACGTG
rabf2b	SALK_090266C	RABF2b_LP TTTGCTTGGTTGGTGAGTTTC RABF2b_RP GCACCGTGTTCAGATAAATCC

References

1. Weiberg A, Wang M, Lin F-M, Zhao H, Zhang Z, Kaloshian I, et al. Fungal small RNAs suppress plant immunity by hijacking host RNA interference pathways. Science. 2013; 342: 118–123. doi: 10.1126/science.1239705.

2. Hua C, Zhao J-H, Guo H-S. Trans-Kingdom RNA Silencing in Plant-Fungal Pathogen Interactions. Mol Plant. 2018; 11: 235–244. doi: 10.1016/j.molp.2017.12.001.

3. Zeng J, Gupta VK, Jiang Y, Yang B, Gong L, Zhu H. Cross-Kingdom Small RNAs among Animals, Plants and Microbes. Cells. 2019; 8. doi: 10.3390/cells8040371.

4. Huang C-Y, Wang H, Hu P, Hamby R, Jin H. Small RNAs - Big Players in Plant-Microbe Interactions. Cell Host Microbe. 2019; 26: 173–182. doi: 10.1016/j.chom.2019.07.021.

5. Koch A, Kogel K-H. New wind in the sails: improving the agronomic value of crop plants through RNAi-mediated gene silencing. Plant Biotechnol J. 2014; 12: 821–831. doi: 10.1111/pbi.12226.

6. Wang M, Weiberg A, Dellota E, Yamane D, Jin H. Botrytis small RNA Bc-siR37 suppresses plant defense genes by cross-kingdom RNAi. RNA Biol. 2017; 14: 421–428. doi: 10.1080/15476286.2017.1291112.

7. Cai Q, He B, Kogel K-H, Jin H. Cross-kingdom RNA trafficking and environmental RNAi-nature's blueprint for modern crop protection strategies. Curr Opin Microbiol. 2018; 46: 58–64. doi: 10.1016/j.mib.2018.02.003.

8. Liu S, Jaouannet M, Dempsey D'MA, Imani J, Coustau C, Kogel K-H. RNA-based technologies for insect control in plant production. Biotechnol Adv. 2019: 107463. doi: 10.1016/j.biotechadv.2019.107463.

9. Waterhouse PM, Graham MW, Wang MB. Virus resistance and gene silencing in plants can be induced by simultaneous expression of sense and antisense RNA. Proc Natl Acad Sci U S A. 1998; 95: 13959–13964. doi: 10.1073/pnas.95.23.13959.

10. Schwind N, Zwiebel M, Itaya A, Ding B, Wang M-B, Krczal G, et al. RNAi-mediated resistance to Potato spindle tuber viroid in transgenic tomato expressing a viroid hairpin RNA construct. Mol Plant Pathol. 2009; 10: 459–469. doi: 10.1111/j.1364-3703.2009.00546.x.

11. Escobar MA, Civerolo EL, Summerfelt KR, Dandekar AM. RNAi-mediated oncogene silencing confers resistance to crown gall tumorigenesis. Proc Natl Acad Sci U S A. 2001; 98: 13437–13442. doi: 10.1073/pnas.241276898.

12. Koch A, Kumar N, Weber L, Keller H, Imani J, Kogel K-H. Host-induced gene silencing of cytochrome P450 lanosterol C14α-demethylase-encoding genes confers strong resistance to Fusarium species. Proc Natl Acad Sci U S A. 2013; 110: 19324–19329. doi: 10.1073/pnas.1306373110.

13. Chen W, Kastner C, Nowara D, Oliveira-Garcia E, Rutten T, Zhao Y, et al. Host-induced silencing of Fusarium culmorum genes protects wheat from infection. J Exp Bot. 2016; 67: 4979–4991. doi: 10.1093/jxb/erw263.

14. Cheng W, Song X-S, Li H-P, Cao L-H, Sun K, Qiu X-L, et al. Host-induced gene silencing of an essential chitin synthase gene confers durable resistance to Fusarium head blight and seedling blight in wheat. Plant Biotechnol J. 2015; 13: 1335–1345. doi: 10.1111/pbi.12352.

15. Panwar V, Jordan M, McCallum B, Bakkeren G. Host-induced silencing of essential genes in Puccinia triticina through transgenic expression of RNAi sequences reduces severity of leaf rust infection in wheat. Plant Biotechnol J. 2018; 16: 1013–1023. doi: 10.1111/pbi.12845.

16. Govindarajulu M, Epstein L, Wroblewski T, Michelmore RW. Host-induced gene silencing inhibits the biotrophic pathogen causing downy mildew of lettuce. Plant Biotechnol J. 2015; 13: 875–883. doi: 10.1111/pbi.12307.

17. Shivakumara TN, Chaudhary S, Kamaraju D, Dutta TK, Papolu PK, Banakar P, et al. Host-Induced Silencing of Two Pharyngeal Gland Genes Conferred Transcriptional Alteration of Cell Wall-Modifying Enzymes of Meloidogyne incognita vis-à-vis Perturbed Nematode Infectivity in Eggplant. Front Plant Sci. 2017; 8: 473. doi: 10.3389/fpls.2017.00473.

18. Chaudhary S, Dutta TK, Tyagi N, Shivakumara TN, Papolu PK, Chobhe KA, et al. Host-induced silencing of Mi-msp-1 confers resistance to root-knot nematode Meloidogyne incognita in eggplant. Transgenic Res. 2019; 28: 327–340. doi: 10.1007/s11248-019-00126-5.

19. Abdellatef E, Will T, Koch A, Imani J, Vilcinskas A, Kogel K-H. Silencing the expression of the salivary sheath protein causes transgenerational feeding suppression in the aphid Sitobion avenae. Plant Biotechnol J. 2015; 13: 849–857. doi: 10.1111/pbi.12322.

20. Coleman AD, Wouters RHM, Mugford ST, Hogenhout SA. Persistence and transgenerational effect of plant-mediated RNAi in aphids. J Exp Bot. 2015; 66: 541–548. doi: 10.1093/jxb/eru450.

21. Mitter N, Worrall EA, Robinson KE, Li P, Jain RG, Taochy C, et al. Clay nanosheets for topical delivery of RNAi for sustained protection against plant viruses. Nat Plants. 2017; 3: 16207. doi: 10.1038/nplants.2016.207.

22. Cai Q, Qiao L, Wang M, He B, Lin F-M, Palmquist J, et al. Plants send small RNAs in extracellular vesicles to fungal pathogen to silence virulence genes. Science. 2018; 360: 1126–1129. doi: 10.1126/science.aar4142.

23. Dubrovina AS, Kiselev KV. Exogenous RNAs for Gene Regulation and Plant Resistance. Int J Mol Sci. 2019; 20. doi: 10.3390/ijms20092282.

24. Dalakouras A, Wassenegger M, Dadami E, Ganopoulos I, Pappas ML, Papadopoulou K. Genetically Modified Organism-Free RNA Interference: Exogenous Application of RNA Molecules in Plants. Plant Physiol. 2020; 182: 38–50. doi: 10.1104/pp.19.00570.

25. Koch A, Biedenkopf D, Furch A, Weber L, Rossbach O, Abdellatef E, et al. An RNAi-Based Control of Fusarium graminearum Infections Through Spraying of Long dsRNAs Involves a Plant Passage and Is Controlled by the Fungal Silencing Machinery. PLoS Pathog. 2016; 12. doi: 10.1371/journal.ppat.1005901.

25. Huvenne H, Smagghe G. Mechanisms of dsRNA uptake in insects and potential of RNAi for pest control: a review. J Insect Physiol. 2010; 56: 227–235. doi: 10.1016/j.jinsphys.2009.10.004.

27. Rutter BD, Innes RW. Extracellular Vesicles Isolated from the Leaf Apoplast Carry Stress-Response Proteins. Plant Physiol. 2017; 173: 728–741. doi: 10.1104/pp.16.01253.

28. Rutter BD, Innes RW. Extracellular vesicles as key mediators of plant-microbe interactions. Curr Opin Plant Biol. 2018; 44: 16–22. doi: 10.1016/j.pbi.2018.01.008.

29. An Q, Ehlers K, Kogel K-H, van Bel AJE, Hückelhoven R. Multivesicular compartments proliferate in susceptible and resistant MLA12-barley leaves in response to infection by the biotrophic powdery mildew fungus. New Phytol. 2006; 172: 563–576. doi: 10.1111/j.1469-8137.2006.01844.x.

30. An Q, Hückelhoven R, Kogel K-H, van Bel AJE. Multivesicular bodies participate in a cell wall-associated defence response in barley leaves attacked by the pathogenic powdery mildew fungus. Cell Microbiol. 2006; 8: 1009–1019. doi: 10.1111/j.1462-5822.2006.00683.x.

31. Albuquerque PC, Nakayasu ES, Rodrigues ML, Frases S, Casadevall A, Zancope-Oliveira RM, et al. Vesicular transport in Histoplasma capsulatum: an effective mechanism for trans-cell wall transfer of proteins and lipids in ascomycetes. Cell Microbiol. 2008; 10: 1695–1710. doi: 10.1111/j.1462-5822.2008.01160.x.

32. Gould SJ, Raposo G. As we wait: coping with an imperfect nomenclature for extracellular vesicles. J Extracell Vesicles. 2013; 2. doi: 10.3402/jev.v2i0.20389.

33. Liégeois S, Benedetto A, Garnier J-M, Schwab Y, Labouesse M. The V0-ATPase mediates apical secretion of exosomes containing Hedgehog-related proteins in Caenorhabditis elegans. J Cell Biol. 2006; 173: 949–961. doi: 10.1083/jcb.200511072.

34. György B, Szabó TG, Pásztói M, Pál Z, Misják P, Aradi B, et al. Membrane vesicles, current state-of-the-art: emerging role of extracellular vesicles. Cell Mol Life Sci. 2011; 68: 2667–2688. doi: 10.1007/s00018-011-0689-3.

35. van der Pol E, Böing AN, Harrison P, Sturk A, Nieuwland R. Classification, functions, and clinical relevance of extracellular vesicles. Pharmacol Rev. 2012; 64: 676–705. doi: 10.1124/pr.112.005983.

36. Akers JC, Gonda D, Kim R, Carter BS, Chen CC. Biogenesis of extracellular vesicles (EV): exosomes, microvesicles, retrovirus-like vesicles, and apoptotic bodies. J Neurooncol. 2013; 113: 1–11. doi: 10.1007/s11060-013-1084-8.

37. Colombo M, Raposo G, Théry C. Biogenesis, secretion, and intercellular interactions of exosomes and other extracellular vesicles. Annu Rev Cell Dev Biol. 2014; 30: 255–289. doi: 10.1146/annurev-cellbio-101512-122326.

38. Pegtel DM, Cosmopoulos K, Thorley-Lawson DA, van Eijndhoven MAJ, Hopmans ES, Lindenberg JL, et al. Functional delivery of viral miRNAs via exosomes. Proc Natl Acad Sci U S A. 2010; 107: 6328–6333. doi: 10.1073/pnas.0914843107.

39. Mittelbrunn M, Gutiérrez-Vázquez C, Villarroya-Beltri C, González S, Sánchez-Cabo F, González MÁ, et al. Unidirectional transfer of microRNA-loaded exosomes from T cells to antigen-presenting cells. Nat Commun. 2011; 2: 282-. doi: 10.1038/ncomms1285.

40. Ridder K, Keller S, Dams M, Rupp A-K, Schlaudraff J, Del Turco D, et al. Extracellular Vesicle-Mediated Transfer of Genetic Information between the Hematopoietic System and the Brain in Response to Inflammation. PLoS Biol. 2014; 12. doi: 10.1371/journal.pbio.1001874.

41. Halperin W, Jensen WA. Ultrastructural changes during growth and embryogenesis in carrot cell cultures. J Ultrastruct Res. 1967; 18: 428–443. doi: 10.1016/s0022-5320(67)80128-x.

42. Xu H, Mendgen K. Endocytosis of 1,3-?-glucans by broad bean cells at the penetration site of the cowpea rust fungus (haploid stage). Planta. 1994; 195. doi: 10.1007/bf00199688.

43. Micali CO, Neumann U, Grunewald D, Panstruga R, O'Connell R. Biogenesis of a specialized plant-fungal interface during host cell internalization of Golovinomyces orontii haustoria. Cell Microbiol. 2011; 13: 210–226. doi: 10.1111/j.1462-5822.2010.01530.x.

44. Stein M, Dittgen J, Sánchez-Rodríguez C, Hou B-H, Molina A, Schulze-Lefert P, et al. Arabidopsis PEN3/PDR8, an ATP binding cassette transporter, contributes to nonhost resistance to inappropriate pathogens that enter by direct penetration. Plant Cell. 2006; 18: 731–746. doi: 10.1105/tpc.105.038372.

45. Petersen KE, Manangon E, Hood JL, Wickline SA, Fernandez DP, Johnson WP, et al. A review of exosome separation techniques and characterization of B16-F10 mouse melanoma exosomes with AF4-UV-MALS-DLS-TEM. Anal Bioanal Chem. 2014; 406: 7855–7866. doi: 10.1007/s00216-014-8040-0.

46. Caillaud M-C, Wirthmueller L, Sklenar J, Findlay K, Piquerez SJM, Jones AME, et al. The plasmodesmal protein PDLP1 localises to haustoria-associated membranes during downy mildew infection and regulates callose deposition. PLoS Pathog. 2014; 10: e1004496. doi: 10.1371/journal.ppat.1004496.

47. Koch A, Stein E, Kogel K-H. RNA-based disease control as a complementary measure to fight Fusarium fungi through silencing of the azole target Cytochrome P450 Lanosterol C-14 α-Demethylase. Eur J Plant Pathol. 2018; 152: 1003–1010. doi: 10.1007/s10658-018-1518-4.

48. Zhang L, Hou D, Chen X, Li D, Zhu L, Zhang Y, et al. Exogenous plant MIR168a specifically targets mammalian LDLRAP1: evidence of cross-kingdom regulation by microRNA. Cell Res. 2012; 22: 107–126. doi: 10.1038/cr.2011.158.

49. Zhang T, Zhao Y-L, Zhao J-H, Wang S, Jin Y, Chen Z-Q, et al. Cotton plants export microRNAs to inhibit virulence gene expression in a fungal pathogen. Nat Plants. 2016; 2: 16153. doi: 10.1038/nplants.2016.153.

50. Wang B, Sun Y, Song N, Zhao M, Liu R, Feng H, et al. Puccinia striiformis f. sp. tritici microRNA-like RNA 1 (Pst-milR1), an important pathogenicity factor of Pst, impairs wheat resistance to Pst by suppressing the wheat pathogenesis-related 2 gene. New Phytol. 2017; 215: 338–350. doi: 10.1111/nph.14577.

51. Wang M, Thomas N, Jin H. Cross-kingdom RNA trafficking and environmental RNAi for powerful innovative pre- and post-harvest plant protection. Curr Opin Plant Biol. 2017; 38: 133–141. doi: 10.1016/j.pbi.2017.05.003.

52. Zhu K, Liu M, Fu Z, Zhou Z, Kong Y, Liang H, et al. Plant microRNAs in larval food regulate honeybee caste development. PLoS Genet. 2017; 13: e1006946. doi: 10.1371/journal.pgen.1006946.

53. Dubey H, Kiran K, Jaswal R, Jain P, Kayastha AM, Bhardwaj SC, et al. Discovery and profiling of small RNAs from Puccinia triticina by deep sequencing and identification of their potential targets in wheat. Funct Integr Genomics. 2019; 19: 391–407. doi: 10.1007/s10142-018-00652-1.

54. Zanini S, Šečić E, Busche T, Kalinowski J, Kogel K-H. Discovery of interaction-related sRNAs and their targets in the Brachypodium distachyon and Magnaporthe oryzae pathosystem; 2019.

55. Dunker F, Trutzenberg A, Rothenpieler JS, Kuhn S, Pröls R, Schreiber T, et al. Oomycete small RNAs invade the plant RNA-induced silencing complex for virulence; 2019.

56. Biedenkopf D, Will T, Knauer T, Jelonek L, Furch ACU, Busche T, et al. Phloem-mediated spreading of SIGS-derived non-coding RNAs in Hordeum vulgare; 2019.

57. Nowara D, Gay A, Lacomme C, Shaw J, Ridout C, Douchkov D, et al. HIGS: Host-Induced Gene Silencing in the Obligate Biotrophic Fungal Pathogen Blumeria graminisWOA. Plant Cell. 2010; 22: 3130–3141. doi: 10.1105/tpc.110.077040.

58. Ghag SB. Host induced gene silencing, an emerging science to engineer crop resistance against harmful plant pathogens. Physiological and Molecular Plant Pathology. 2017; 100: 242–254. doi: 10.1016/j.pmpp.2017.10.003.

59. Gaffar FY, Koch A. Catch Me If You Can! RNA Silencing-Based Improvement of Antiviral Plant Immunity. Viruses. 2019; 11. doi: 10.3390/v11070673.

60. Peres da Silva R, Puccia R, Rodrigues ML, Oliveira DL, Joffe LS, César GV, et al. Extracellular vesicle-mediated export of fungal RNA. Sci Rep. 2015; 5: 7763. doi: 10.1038/srep07763.

61. Ratajczak J, Wysoczynski M, Hayek F, Janowska-Wieczorek A, Ratajczak MZ. Membrane-derived microvesicles: important and underappreciated mediators of cell-to-cell communication. Leukemia. 2006; 20: 1487–1495. doi: 10.1038/sj.leu.2404296.

62. Valadi H, Ekström K, Bossios A, Sjöstrand M, Lee JJ, Lötvall JO. Exosome-mediated transfer of mRNAs and microRNAs is a novel mechanism of genetic exchange between cells. Nat Cell Biol. 2007; 9: 654–659. doi: 10.1038/ncb1596.

63. Takahashi R-U, Prieto-Vila M, Hironaka A, Ochiya T. The role of extracellular vesicle microRNAs in cancer biology. Clin Chem Lab Med. 2017; 55: 648–656. doi: 10.1515/cclm-2016-0708.

64. Maia J, Caja S, Strano Moraes MC, Couto N, Costa-Silva B. Exosome-Based Cell-Cell Communication in the Tumor Microenvironment. Front Cell Dev Biol. 2018; 6: 18. doi: 10.3389/fcell.2018.00018.

65. Mu J, Zhuang X, Wang Q, Jiang H, Deng Z-B, Wang B, et al. Interspecies communication between plant and mouse gut host cells through edible plant derived exosome-like nanoparticles. Mol Nutr Food Res. 2014; 58: 1561–1573. doi: 10.1002/mnfr.201300729.

66. Raposo G, Stoorvogel W. Extracellular vesicles: Exosomes, microvesicles, and friends. J Cell Biol. 2013; 200: 373–383. doi: 10.1083/jcb.201211138.

67. Li P, Kaslan M, Lee SH, Yao J, Gao Z. Progress in Exosome Isolation Techniques. Theranostics. 2017; 7: 789–804. doi: 10.7150/thno.18133.

68. Szatanek R, Baran J, Siedlar M, Baj-Krzyworzeka M. Isolation of extracellular vesicles: Determining the correct approach (Review). Int J Mol Med. 2015; 36: 11–17. doi: 10.3892/ijmm.2015.2194.

69. van Balkom BWM, Eisele AS, Pegtel DM, Bervoets S, Verhaar MC. Quantitative and qualitative analysis of small RNAs in human endothelial cells and exosomes provides insights into localized RNA processing, degradation and sorting. J Extracell Vesicles. 2015; 4: 26760. doi: 10.3402/jev.v4.26760.

70. Alexander RP, Chiou N-T, Ansel KM. Improved exosome isolation by sucrose gradient fractionation of ultracentrifuged crude exosome pellets. Protocol Exchange. 2016. doi: 10.1038/protex.2016.057.

71. Höfle L, Biedenkopf D, Werner BT, Shrestha A, Jelonek L, Koch A. Study on the efficiency of dsRNAs with increasing length in RNA-based silencing of the Fusarium CYP51 genes. RNA Biol. 2020: 1–11. doi: 10.1080/15476286.2019.1700033.

72. Wang F, Shang Y, Fan B, Yu J-Q, Chen Z. Arabidopsis LIP5, a Positive Regulator of Multivesicular Body Biogenesis, Is a Critical Target of Pathogen-Responsive MAPK Cascade in Plant Basal Defense. PLoS Pathog. 2014; 10. doi: 10.1371/journal.ppat.1004243.

73. Meyer D, Pajonk S, Micali C, O'Connell R, Schulze-Lefert P. Extracellular transport and integration of plant secretory proteins into pathogen-induced cell wall compartments. Plant J. 2009; 57: 986–999. doi: 10.1111/j.1365-313X.2008.03743.x.

74. Regente M, Pinedo M, San Clemente H, Balliau T, Jamet E, La Canal L de. Plant extracellular vesicles are incorporated by a fungal pathogen and inhibit its growth. J Exp Bot. 2017; 68: 5485–5495. doi: 10.1093/jxb/erx355.

75. Quintana JF, Babayan SA, Buck AH. Small RNAs and extracellular vesicles in filarial nematodes: From nematode development to diagnostics. Parasite Immunol. 2017; 39. doi: 10.1111/pim.12395.

76. Katsir L, Bahar O. Bacterial outer membrane vesicles at the plant–pathogen interface. PLoS Pathog. 2017; 13. doi: 10.1371/journal.ppat.1006306.

77. Buck AH, Coakley G, Simbari F, McSorley HJ, Quintana JF, Le Bihan T, et al. Exosomes secreted by nematode parasites transfer small RNAs to mammalian cells and modulate innate immunity. Nat Commun. 2014; 5: 5488. doi: 10.1038/ncomms6488.

78. Zhu L, Liu J, Dao J, Lu K, Li H, Gu H, et al. Molecular characterization of S. japonicum exosome-like vesicles reveals their regulatory roles in parasite-host interactions. Sci Rep. 2016; 6: 25885. doi: 10.1038/srep25885.

79. Henne WM, Stenmark H, Emr SD. Molecular Mechanisms of the Membrane Sculpting ESCRT Pathway. Cold Spring Harb Perspect Biol. 2013; 5. doi: 10.1101/cshperspect.a016766.

80. Lazo GR, Stein PA, Ludwig RA. A DNA transformation-competent Arabidopsis genomic library in Agrobacterium. Biotechnology (N Y). 1991; 9: 963–967. doi: 10.1038/nbt1091-963.

81. Bechtold N, Pelletier G. In planta Agrobacterium-mediated transformation of adult Arabidopsis thaliana plants by vacuum infiltration. Methods Mol Biol. 1998; 82: 259–266. doi: 10.1385/0-89603-391-0:259.

82. Martin M. Cutadapt removes adapter sequences from high-throughput sequencing reads. EMBnet j. 2011; 17: 10. doi: 10.14806/ej.17.1.200.

83. Langmead B, Salzberg SL. Fast gapped-read alignment with Bowtie 2. Nat Methods. 2012; 9: 357–359. doi: 10.1038/nmeth.1923.

84. Quinlan AR, Hall IM. BEDTools: a flexible suite of utilities for comparing genomic features. Bioinformatics. 2010; 26: 841–842. doi: 10.1093/bioinformatics/btq033.

85. Kent WJ, Zweig AS, Barber G, Hinrichs AS, Karolchik D. BigWig and BigBed : enabling browsing of large distributed datasets. 26, 2204–2207 (2010).

86. Thorvaldsdóttir H, Robinson JT, Mesirov JP. Integrative Genomics Viewer (IGV): high-performance genomics data visualization and exploration. Brief Bioinformatics. 2013; 14: 178–192. doi: 10.1093/bib/bbs017.

87. Vannuruswamy G, Korwar AM, Jagadeeshaprasad MG, Kulkarni MJ. Targeted Quantification of the Glycated Peptides of Human Serum Albumin. Methods Mol Biol. 2017; 1619: 403–416. doi: 10.1007/978-1-4939-7057-5_28.

88. Korwar AM, Vannuruswamy G, Jagadeeshaprasad MG, Jayaramaiah RH, Bhat S, Regin BS, et al. Development of Diagnostic Fragment Ion Library for Glycated Peptides of Human Serum Albumin: Targeted Quantification in Prediabetic, Diabetic, and Microalbuminuria Plasma by Parallel Reaction Monitoring, SWATH, and MSE*. Mol Cell Proteomics. 2015; 14: 2150–2159. doi: 10.1074/mcp.M115.050518.

Figures

Koch et al. 2020

Figure 1

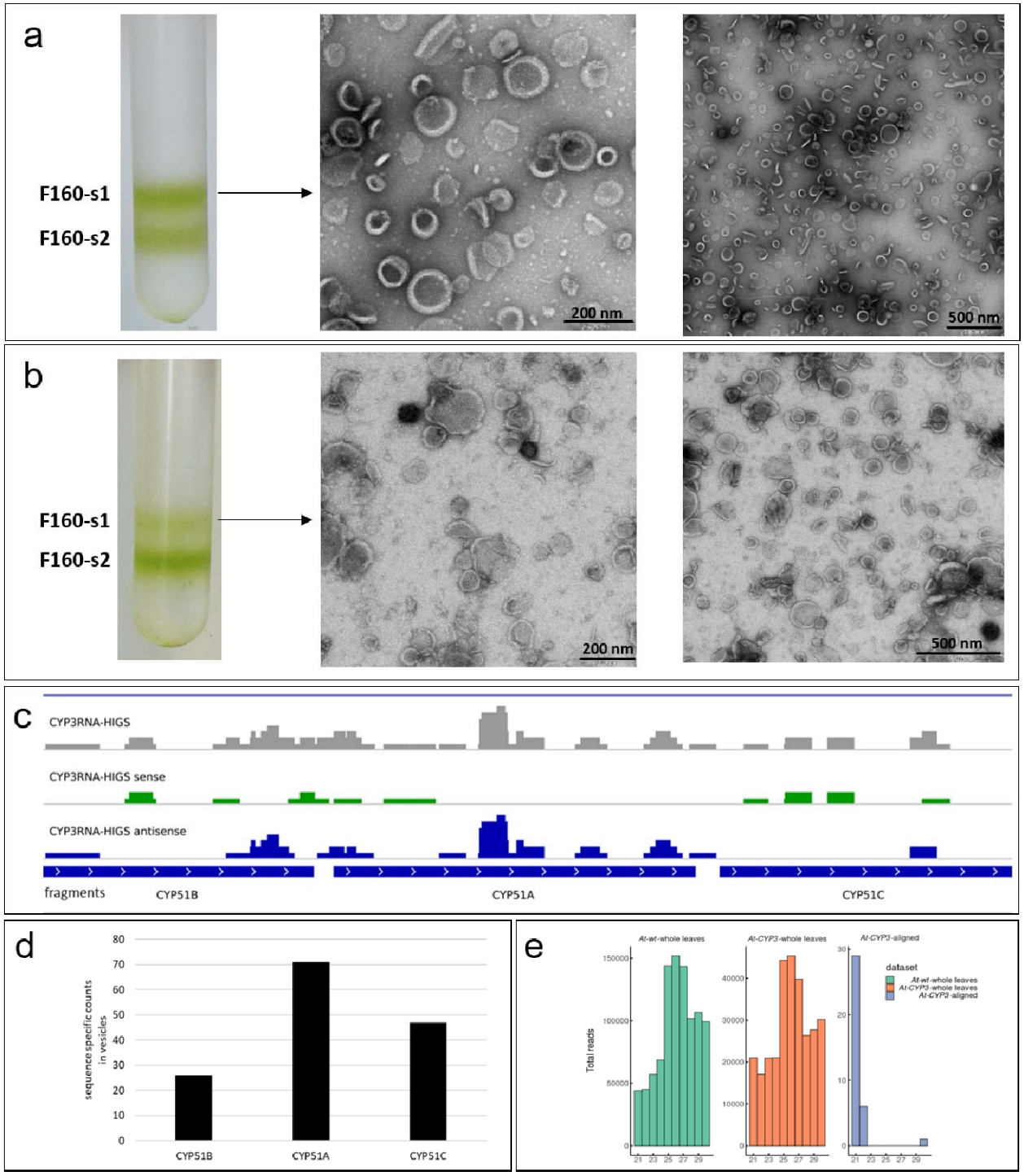
a
F160-s1
F160-s2
200 nm
500 nm
b
F160-s1
F160-s2
200 nm
500 nm
c
CYP3RNA-HIGS
CYP3RNA-HIGS sense
CYP3RNA-HIGS antisense
fragments
CYP51B
CYP51A
CYP51C
d
sequence specific counts in vesicles
0
10
20
30
40
50
60
70
80
CYP51B
CYP51A
CYP51C
e
At-wt-whole leaves
At-CYP3-whole leaves
At-CYP3-aligned
Total reads
dataset
At-wt-whole leaves
At-CYP3-whole leaves
At-CYP3-aligned

Figure 2

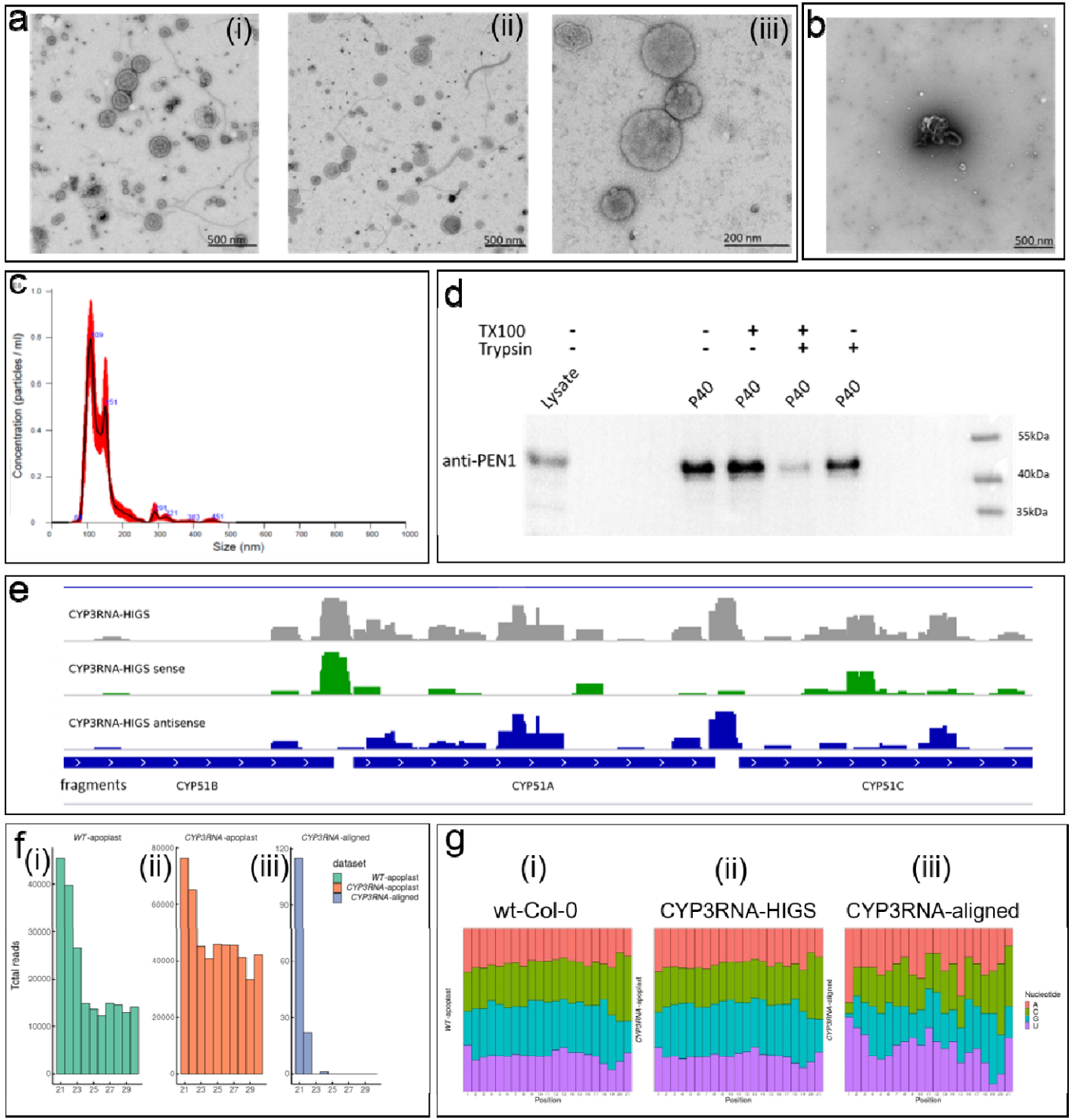
a
(i)
(ii)
(iii)
500 nm
500 nm
200 nm
b
500 nm
c
Concentration (particles / ml)
Size (nm)
d
TX100
Trypsin
Lysate
P40
P40
P40
P40
anti-PEN1
55kDa
40kDa
35kDa
e
CYP3RNA-HIGS
CYP3RNA-HIGS sense
CYP3RNA-HIGS antisense
fragments
CYP51B
CYP51A
CYP51C
f
(i)
(ii)
(iii)
WT-apoplast
CYP3RNA-apoplast
CYP3RNA-aligned
dataset
Total reads
g
(i)
(ii)
(iii)
wt-Col-0
CYP3RNA-HIGS
CYP3RNA-aligned
Position
Nucleotide

Figure 3

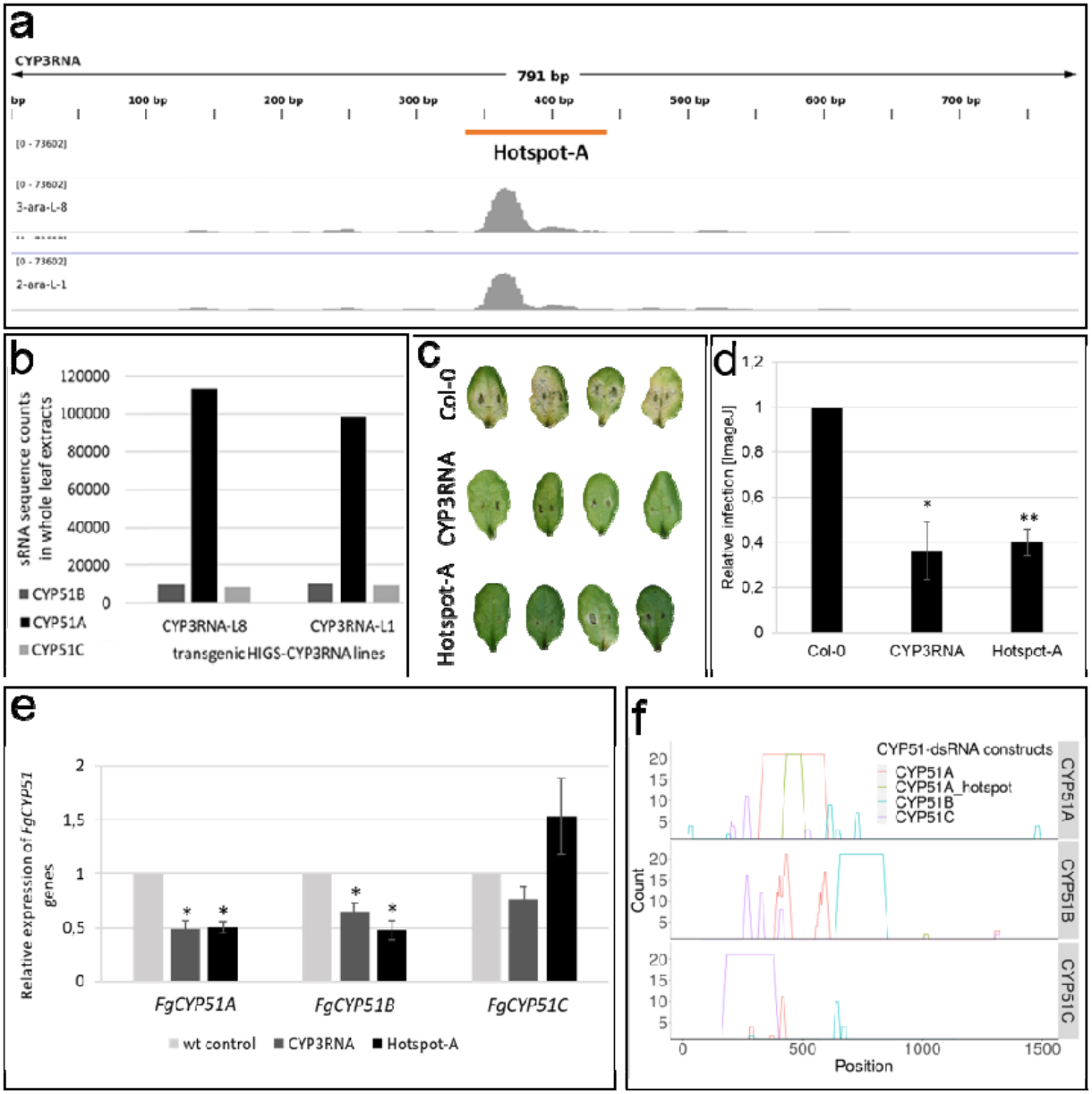
a
CYP3RNA
791 bp
bp
100 bp
200 bp
300 bp
400 bp
500 bp
600 bp
700 bp
[0 - 73602]
Hotspot-A
[0 - 73602]
3-ara-L-8
[0 - 73602]
2-ara-L-1
b
sRNA sequence counts in whole leaf extracts
120000
100000
80000
60000
40000
20000
0
CYP51B
CYP51A
CYP51C
CYP3RNA-L8
CYP3RNA-L1
transgenic HIGS-CYP3RNA lines
c
Col-0
CYP3RNA
Hotspot-A
d
Relative infection [ImageJ]
1,2
1
0,8
0,6
0,4
0,2
0
*
**
Col-0
CYP3RNA
Hotspot-A
e
Relative expression of FgCYP51 genes
2
1,5
1
0,5
0
*
*
*
*
FgCYP51A
FgCYP51B
FgCYP51C
wt control
CYP3RNA
Hotspot-A
f
CYP51-dsRNA constructs
CYP51A
CYP51A_hotspot
CYP51B
CYP51C
Count
20
15
10
5
CYP51A
CYP51B
CYP51C
0
500
1000
1500
Position

Figure 4

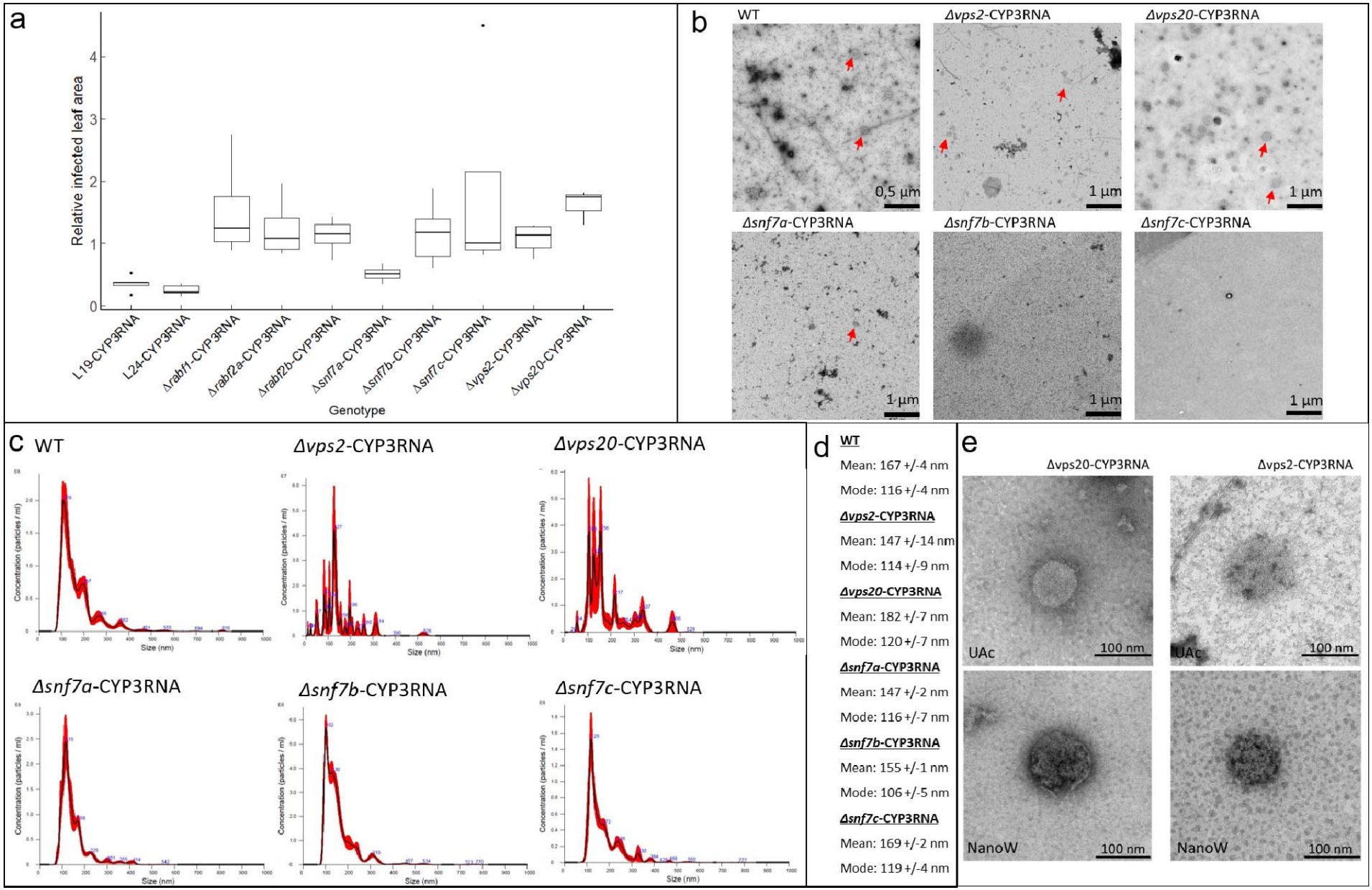
a
Relative infected leaf area
0
1
2
3
4
L19-CYP3RNA
L24-CYP3RNA
Δrabf1-CYP3RNA
Δrabf2a-CYP3RNA
Δrabf2b-CYP3RNA
Δsnf7a-CYP3RNA
Δsnf7b-CYP3RNA
Δsnf7c-CYP3RNA
Δvps2-CYP3RNA
Δvps20-CYP3RNA
Genotype
b
WT
Δvps2-CYP3RNA
Δvps20-CYP3RNA
0,5 µm
1 µm
1 µm
Δsnf7a-CYP3RNA
Δsnf7b-CYP3RNA
Δsnf7c-CYP3RNA
1 µm
1 µm
1 µm
c
WT
Δvps2-CYP3RNA
Δvps20-CYP3RNA
Δsnf7a-CYP3RNA
Δsnf7b-CYP3RNA
Δsnf7c-CYP3RNA
Concentration (particles / ml)
Size (nm)
d
WT
Mean: 167 +/-4 nm
Mode: 116 +/-4 nm
Δvps2-CYP3RNA
Mean: 147 +/-14 nm
Mode: 114 +/-9 nm
Δvps20-CYP3RNA
Mean: 182 +/-7 nm
Mode: 120 +/-7 nm
Δsnf7a-CYP3RNA
Mean: 147 +/-2 nm
Mode: 116 +/-7 nm
Δsnf7b-CYP3RNA
Mean: 155 +/-1 nm
Mode: 106 +/-5 nm
Δsnf7c-CYP3RNA
Mean: 169 +/-2 nm
Mode: 119 +/-4 nm
e
Δvps20-CYP3RNA
Δvps2-CYP3RNA
UAc
100 nm
UAc
100 nm
NanoW
100 nm
NanoW
100 nm

Figure 5

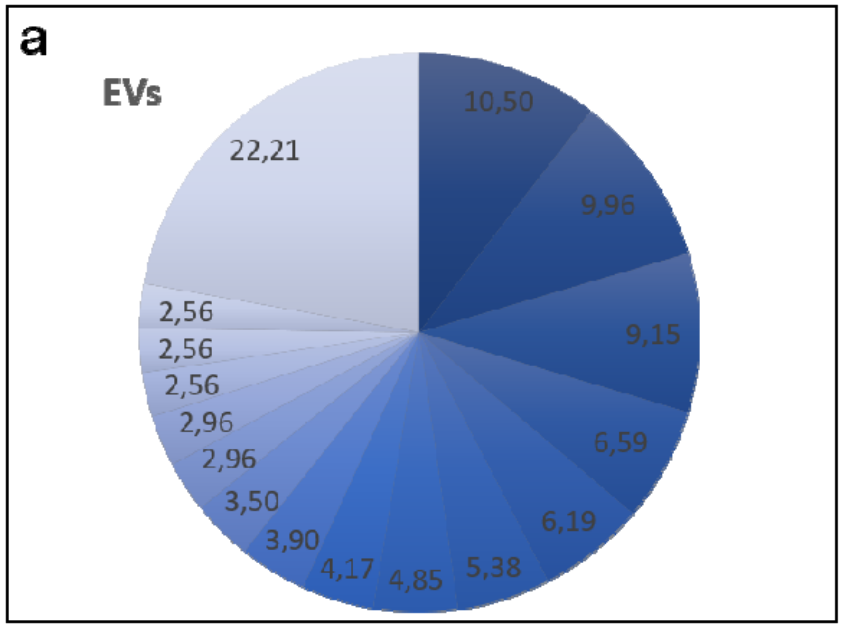

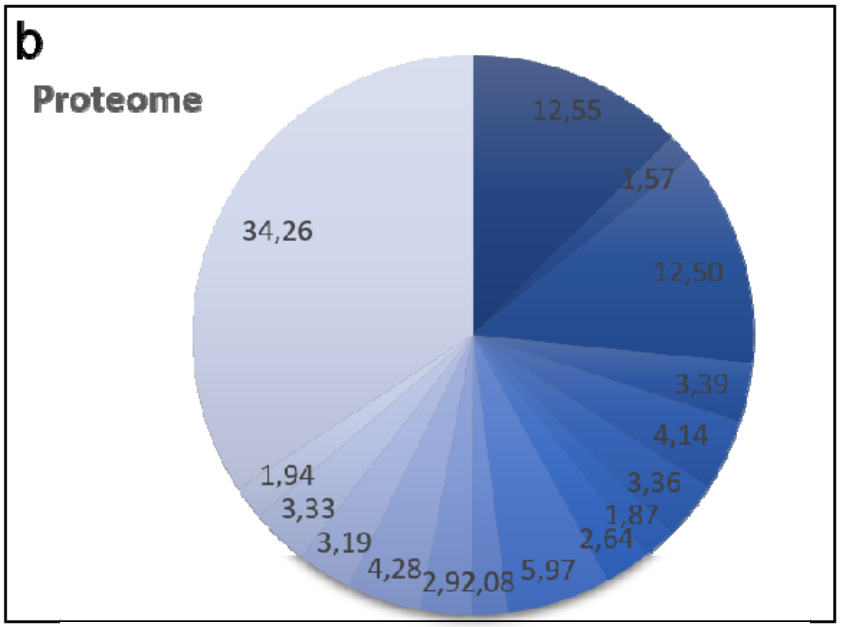

c

GO term (Biological process)	EVs	Proteome
other cellular processes	10.50	12.55
translation	9.56	1.57
other metabolic processes	9.15	12.50
cellular component organization	6.59	3.39
response to stress	6.19	4.14
response to chemical	5.38	3.36
response to abiotic stimulus	4.85	1.87
transport	4.17	2.64
biosynthetic process	3.50	5.97
catabolic process	3.50	2.08
cellular protein modification process	2.56	2.92
nucleobase-containing compound metabolic process	2.56	4.28
anatomical structure development	2.56	3.19
multicellular organism development	2.56	3.33
protein metabolic process	2.56	1.94
other	22.21	34.26

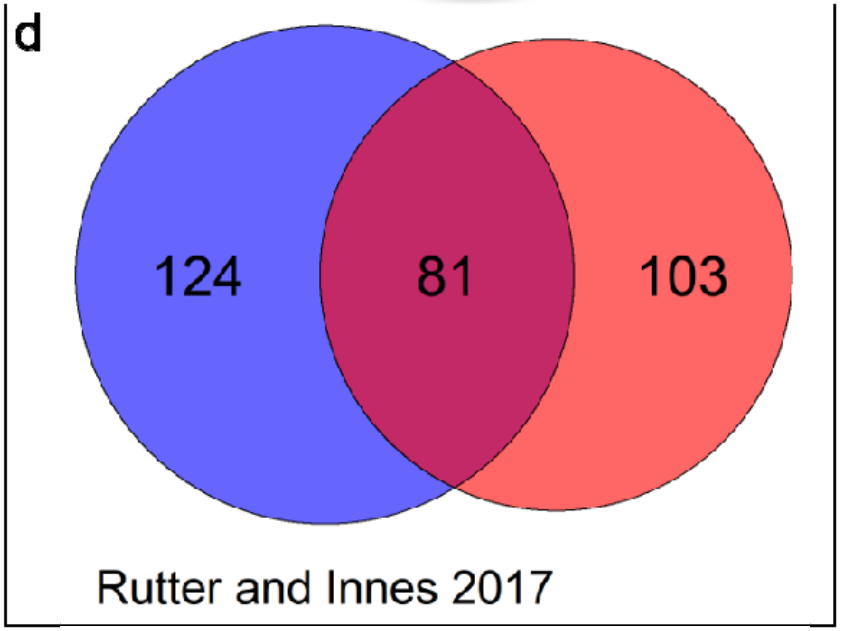

Figure 6

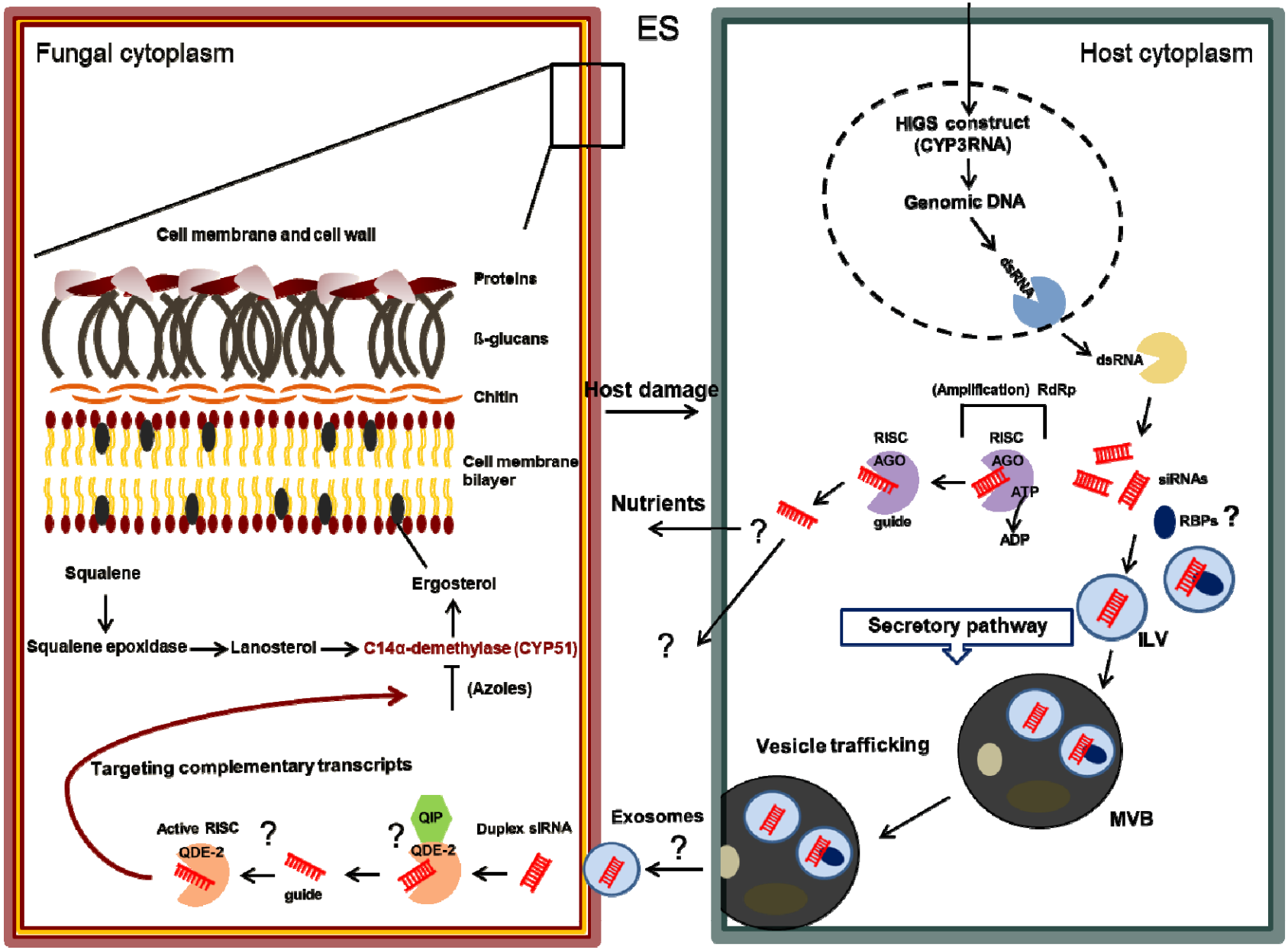
Fungal cytoplasm
ES
Host cytoplasm
Cell membrane and cell wall
Proteins
ß-glucans
Chitin
Cell membrane bilayer
Ergosterol
Squalene
Squalene epoxidase
Lanosterol
C14α-demethylase (CYP51)
(Azoles)
Targeting complementary transcripts
Active RISC
QDE-2
guide
QIP
QDE-2
Duplex siRNA
Host damage
Nutrients
Exosomes
HIGS construct (CYP3RNA)
Genomic DNA
dsRNA
dsRNA
(Amplification) RdRp
RISC
AGO
guide
RISC
AGO
ATP
ADP
siRNAs
RBPs
Secretory pathway
ILV
Vesicle trafficking
MVB

Supplementary Figure 1

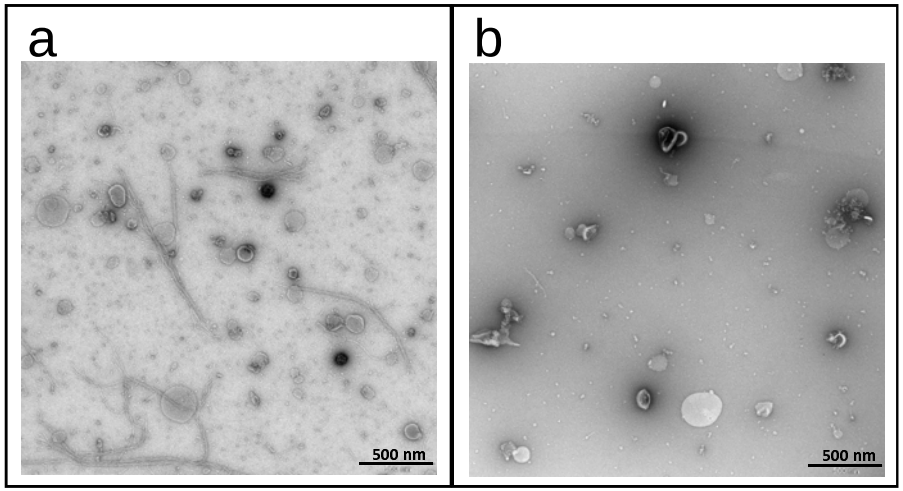

Supplementary Figure 2

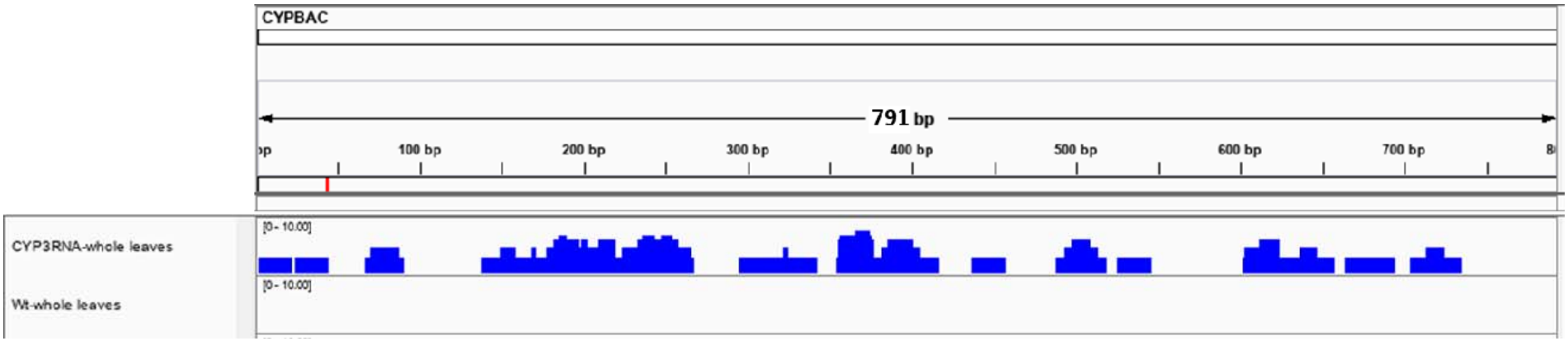

Supplementary Figure 3

Supplementary Figure 3

Supplementary Figure 4

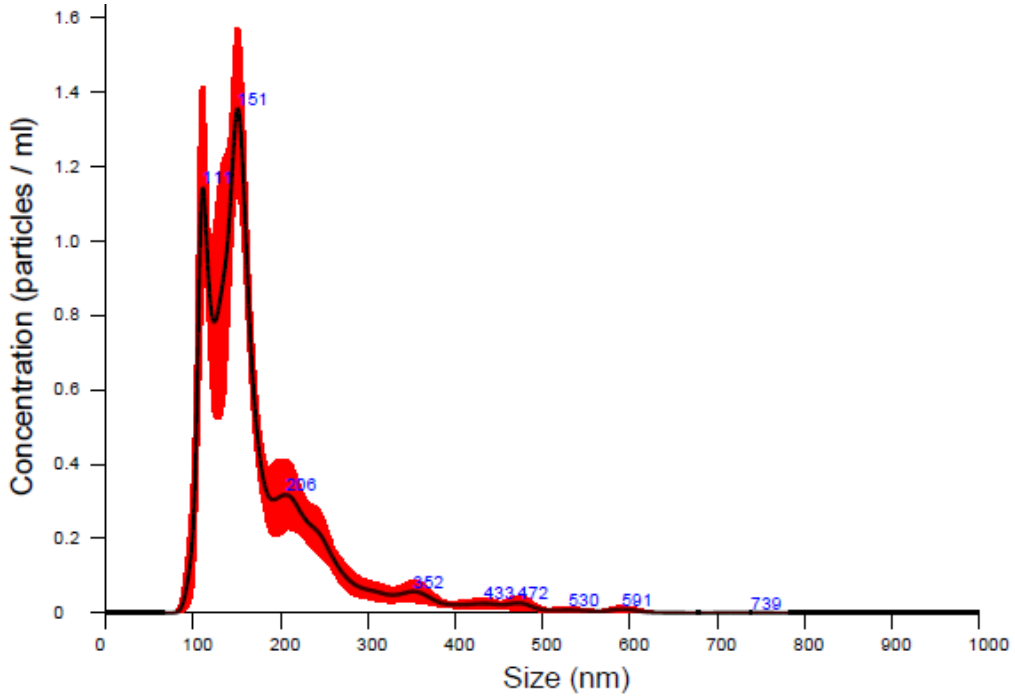

Supplementary Figure 5

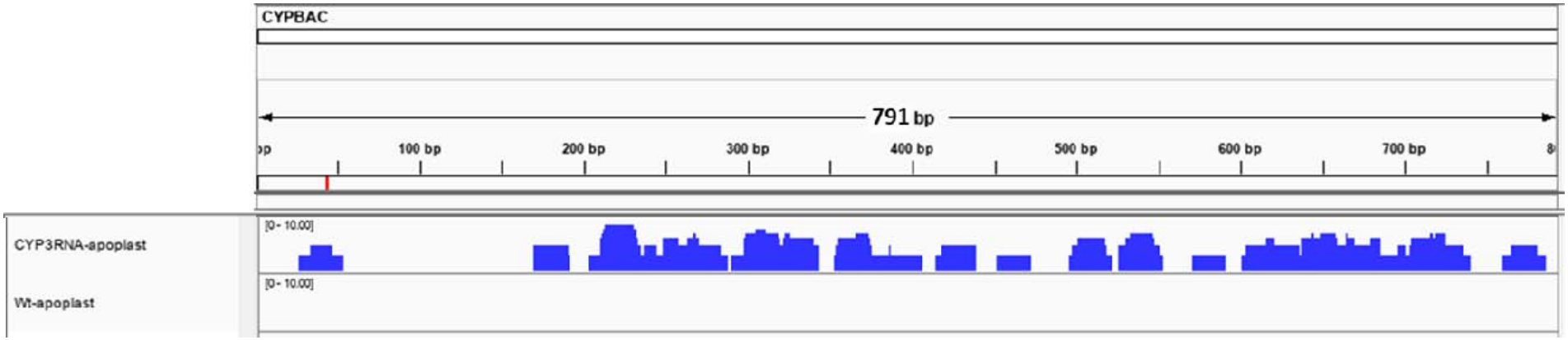

Supplementary Figure 6

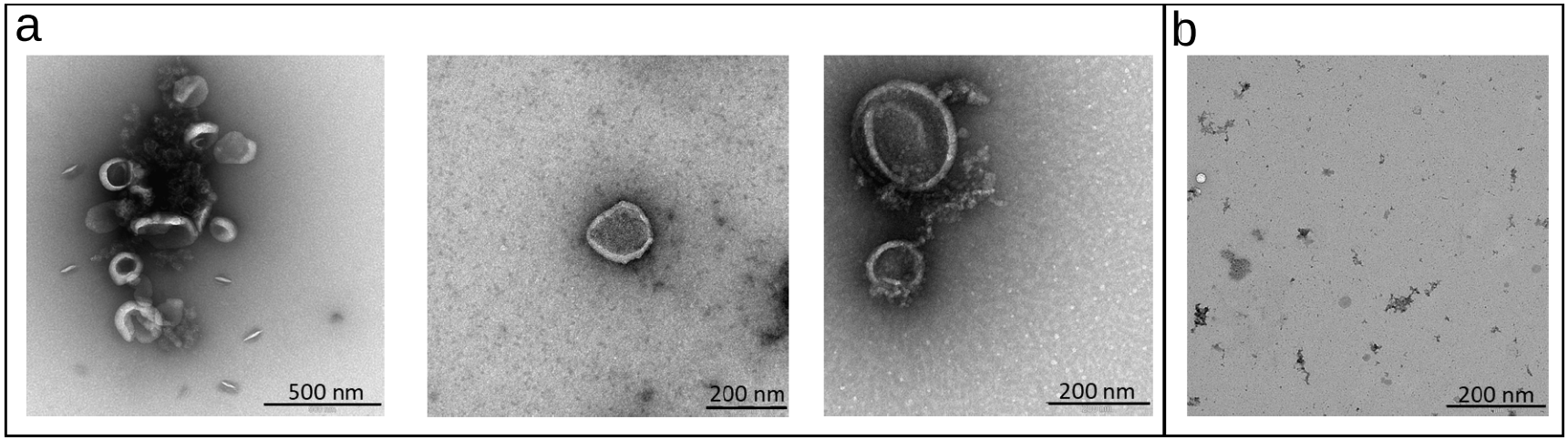

Supplementary Figure 7

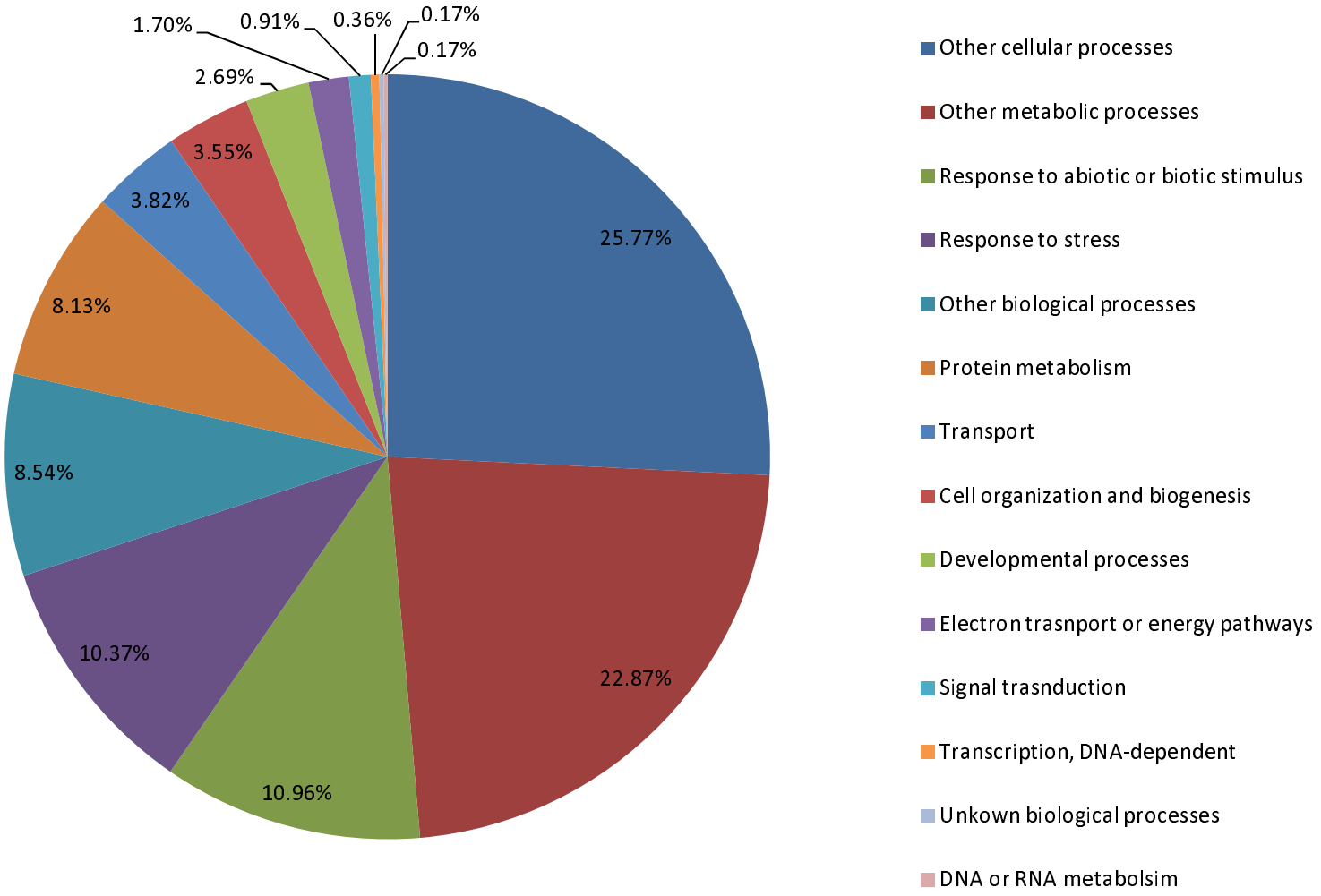

Supplementary Figure 8

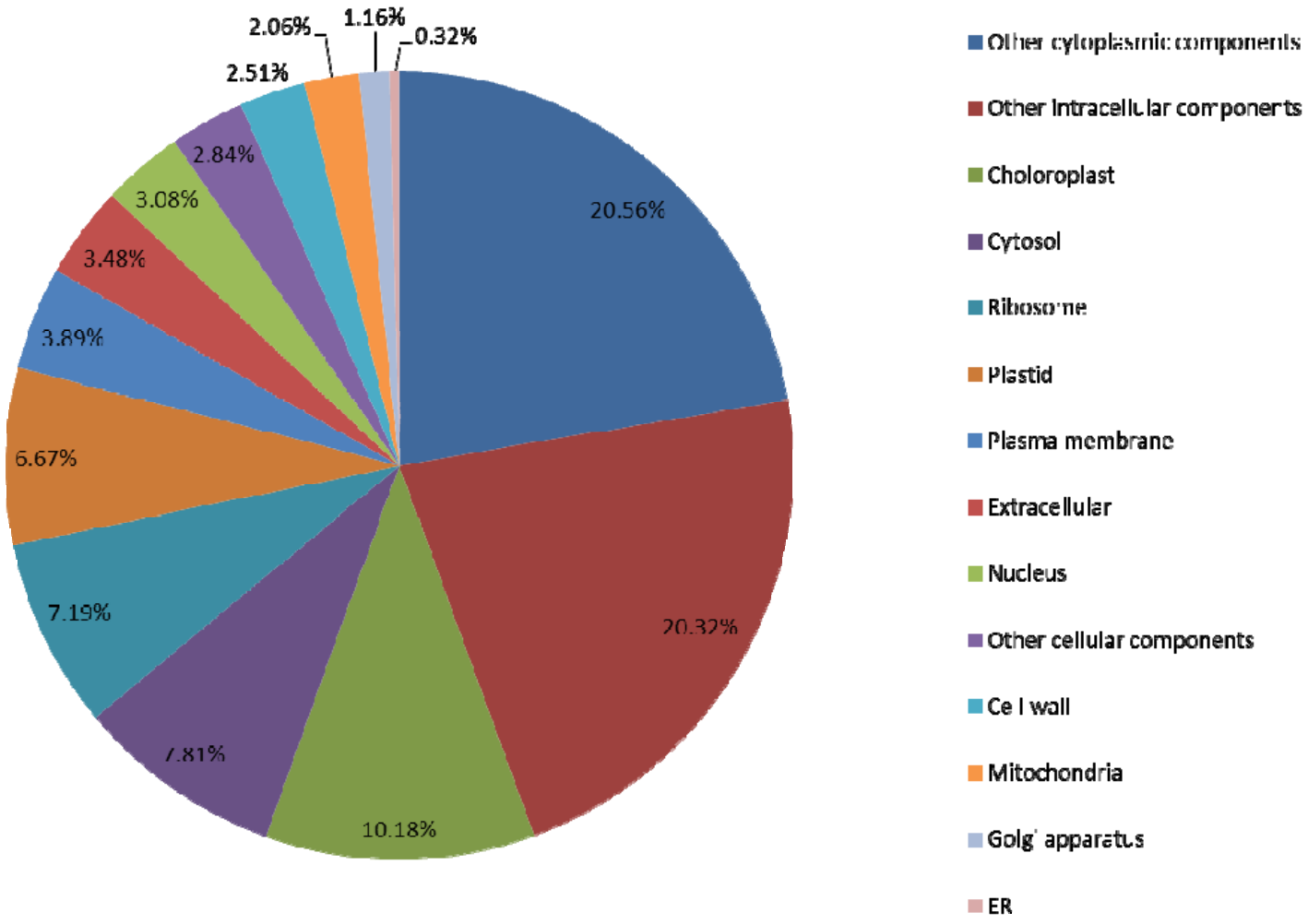

Supplementary Figure 9